IOWA STATE UNIVERSITY
Digital Repository

1962

Adsorption of water vapor by sodium and calcium montmorillonites

Turgut Demirel
Iowa State University

Follow this and additional works at: https://lib.dr.iastate.edu/rtd

Part of the Civil Engineering Commons

ADSORPTION OF WATER VAPOR BY SODIUM

AND CALCIUM MONTMORILLONITES

by

Turgut Demirel

A Dissertation Submitted to the

Graduate Faculty in Partial Fulfillment of

The Requirements for the Degree of

DOCTOR OF PHILOSOPHY

Major Subject: Soil Engineering

Approved:

In Charge of Major Work

Head of Major Department

Dean of Graduate College

Iowa State University
Of Science and Technology
Ames, Iowa

1962

TABLE OF CONTENTS

INTRODUCTION

The load carrying capacity of most soils decreases when subjected to the action of water, the extent of this decrease depending on the type of foundation material. Clay foundations are most susceptible and among clays montmorillonitic type clays are the worst.

The water susceptibility of a montmorillonitic clay varies depending on the kind of associated cation. For instance, sodium montmorillonite is recognized as being more sensitive to water action than calcium montmorillonite. In soil engineering it is generally believed that the weakening action of water on soils is a direct result of the attraction of water molecules by clay mineral particles, sodium montmorillonite having more affinity for water than calcium montmorillonite. It is also generally accepted that clays owe the greater part of their mechanical strength to the water films surrounding individual grains (55). These water films give rise to cohesive forces partly due to surface tension forces at the air/water interface within the clay structure, but in the main due to interactions between the clay particles and water molecules (29, p. 235, 55, 56). Cohesive forces are strongest at relatively low moisture contents and decrease rapidly as the moisture content increases, giving rise to a decrease in the bearing capacity as mentioned above.

The important role that water plays in physical

properties of clays has attracted the attention of many in-
vestigators (27, 28, 30, 37, 38, 44, 59). However, compara-
tively little has been done on the investigation and inter-
pretation of the adsorption isotherms of water vapor on clay
minerals (48, 49, 50, 61). The objective of the present
investigation was to obtain complete vapor adsorption iso-
therms for water with sodium and calcium montmorillonite, and
to deduce information from the adsorption data, namely free
energies of wetting, the area occupied by each molecule of
water, the arrangement of water molecules on clay surface,
and the relative magnitude of the interaction between clay
particles.

THEORY AND REVIEW OF LITERATURE

Bangham was the first to show that Gibbs adsorption equation is applicable to the determination of the free surface energy changes that occur during adsorption of vapors on solid surfaces (3, 4). Other investigators also using Gibbsian methods of approach have shown that the free energy of immersion of a solid surface of unit area in the saturated vapor is calculable from vapor adsorption data (2, 6, 34). The formulae given by these investigators are derivable from each other (35). The equation for the free energy of immersion of a non-porous solid in the saturated vapor, given by Boyd and Livingstone (6) reads:

$$\Delta F = (\gamma_{SL} - \gamma_{SO} + \gamma_{LV}) = - \frac{RT}{M\Sigma} \int_{0}^{p_o} \frac{q}{p}\, dp \qquad (1)$$

where γ_{SL} is the solid-liquid interfacial tension, γ_{SO} is the surface tension of the solid in vacuum, and γ_{LV} is the surface tension of the liquid in contact with its own vapor; q is the mass of vapor adsorbed by the solid of unit mass at pressure p; R, T, M, Σ and p_o are the gas constant, absolute temperature, molecular weight of the vapor, specific surface of the solid and the saturation pressure, respectively.

An independent and simpler derivation of equation 1 will be presented to better elucidate its meaning: With the temperature constant the differential free energy change from transferring saturated vapor onto the solid surface of unit

area in equilibrium with the vapor at pressure p is

$$\frac{\partial \Delta F}{\partial n} = \mu - \mu_o \qquad (2)$$

where ΔF is the free energy change, n is the number of moles of vapor transferred, μ_o is the chemical potential of the saturated vapor and μ is that of the vapor at pressure p. If the vapor is an ideal gas (6), then

$$\mu = \mu_o + RT \ln \frac{p}{p_o} \qquad (3)$$

Let n_o be the number of moles of vapor adsorbed when $\frac{p}{p_o} = 1$; the integral free energy change on transferring saturated vapor onto the solid surface in vacuum until the equilibrium pressure equals the saturation pressure can be obtained from equations 2 and 3:

$$\Delta F = RT \int_0^{n_o} \ln \frac{p}{p_o} \, dn \qquad (4)$$

On the assumption also made by others (2, 3, 4, 6, 34) that the limit of $\frac{n}{p}$ at $p = 0$ is finite, the integration variable can be changed by total differentiation and equation 4 can be put into the following form:

$$\Delta F = - RT \int_0^{p_o} \frac{n}{p} \, dp \qquad (5)$$

Expressing the number of moles, n, of the vapor adsorbed on the unit surface area of the solid in terms of mass:

$$n = \frac{q}{M \Sigma} \qquad (6)$$

and substituting $p_o d \frac{p}{p_o}$ for dp equation 5 can be changed into the following expression:

$$\Delta F = - \frac{RT}{M\Sigma} \int_0^1 \frac{q}{p/p_o} d(p/p_o) \qquad (7)$$

which is a more convenient form of the right hand member of equation 1.

ΔF given by equation 7 is the free energy change accompanying the above mentioned process which is terminated when the equilibrium pressure equals p_o. If the adsorbent used is a mass of non-interacting fine powder, before this final stage is reached, capillary condensation in the contact zones of particles theoretically fills the voids with the liquid, providing that the solid is wettable by the liquid. It follows, therefore, that in such cases

$$\Delta F = \gamma_{SL} - \gamma_{SO} \qquad (8)$$

In other words, calculated ΔF should be the free energy of immersion of a solid surface of unit area in the bulk liquid. This point of view was put forward by Bartell and his co-workers (15, 19, 26) in the case of porous solids and compressed powders of non-porous solids. It has also been shown that the validity of this point of view does not depend on the degree of compression (15). However, some investigators (6, 35), in spite of the fact that the solids investigated are wettable, calculate ΔF by an extrapolation to saturation pressure and identify it with the free energy of immersion in

saturated vapor, assuming that no capillary condensation takes
place. To obtain the free energy of immersion of solids in
the bulk liquid, they make a correction which amounts to
subtracting the surface tension of the liquid from ΔF. This
presumes zero contact angles. The assumption of no capillary
condensation on one hand, and the steepness of the adsorption
isotherm near $p/p_0 = 1$ on the other, introduce uncertainties
into the free energy of immersion determined in this way (15).
For these reasons and because of the porous nature of clay
minerals, particular effort was made to actually reach satu-
ration in the present work, and the free energy of immersion
in bulk liquid was calculated directly from equation 7 by
graphical integration. For interacting solid particles like
clay minerals equation 8 must be modified to introduce another
term representing the particle interaction. The free energy
change ΔF given by equation 7 equals the free energy change
expressed by equation 8 if the solid powder adsorbent has a
rigid structure, uninfluenced by the adsorbate. If the
adsorbate enters the interstices of interacting solid surfaces
causing a separation against the forces of interaction, equa-
tion 8 may be changed, as explained schematically in Figure 1
into the following formulation:

$$\Delta F = (\gamma_{SL} - \gamma_{SO}) + a\, \Delta v \qquad (8a)$$

where a is the interstitial surface area per cm^2 of the total
surface and ΔV is the change in the potential energy of

Figure 1. Schematic representation of the immersion of
interacting solid powders in liquids

        The change from state I to state III is carried in two
ways: through path 1 over an intermediate state II by a
hypothetical isothermal and reversible process, or through
path 2 by isothermal adsorption of the vapor on solid which
has been observed to be thermodynamically reversible (10).

$\Delta F_{II} = \gamma_{SL} - \gamma_{SO}$

Path I

$\Delta F_{I} = \alpha \Delta V$

Vacuum

II

Vacuum

I

$\Delta F = \Delta F_{I} + \Delta F_{II} = \gamma_{SL} - \gamma_{SO} + \alpha \Delta V$

Path 2

Liquid

III
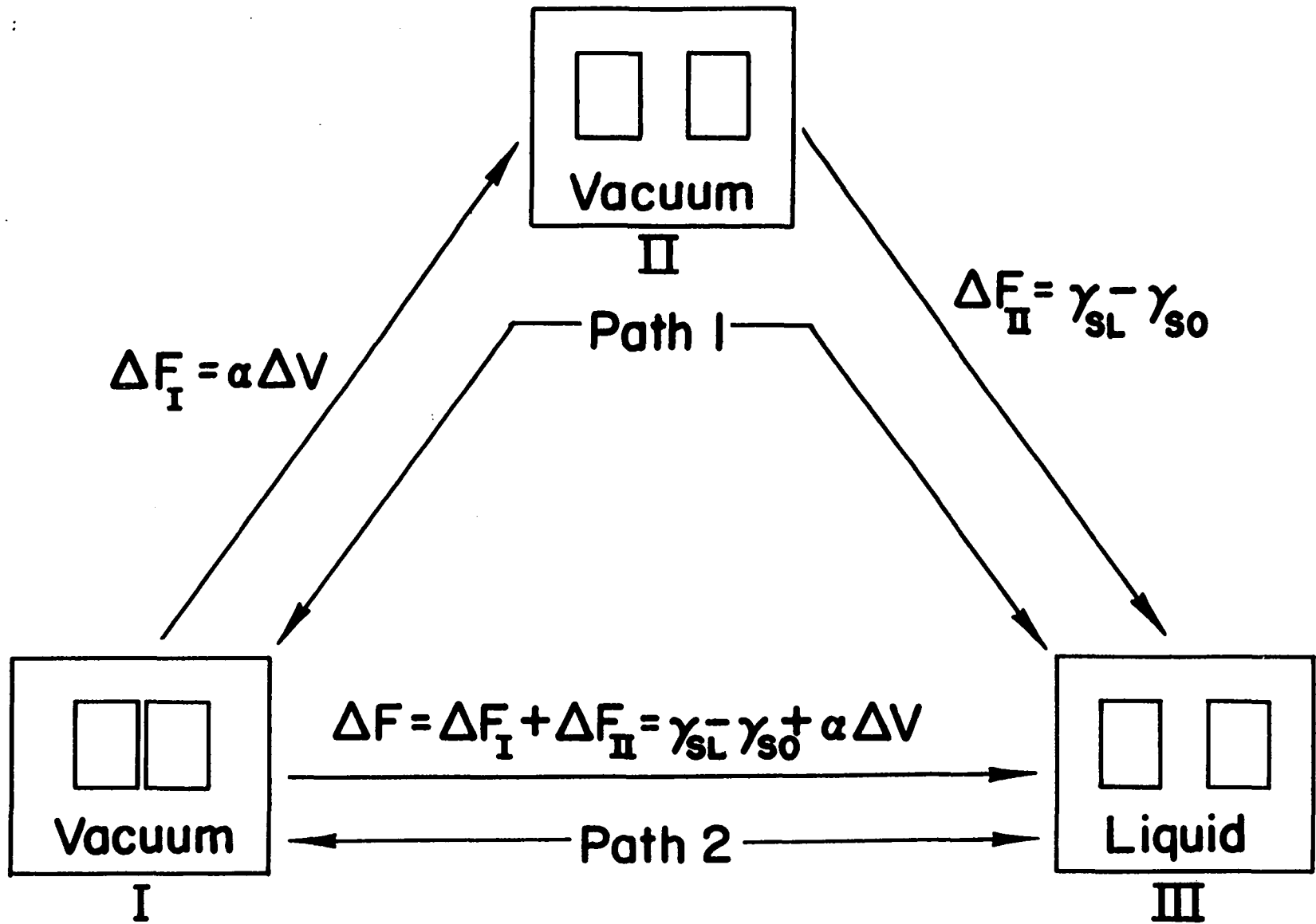
interaction or the free energy change per cm^2 of the inter-
sticial surface due to the separation of particles against
the force of interaction (52, p. 253). Therefore, in case of
clay minerals the free energy change given by equation 7 would
be equivalent to the free energy change expressed by equation
8a. In this study the bracketed first term of the right hand
side of this equation will be referred to as the free energy
of immersion of the solid in the liquid and ΔF as _free energy_
of wetting of the solid by the liquid.

Brunauer et al. (10, 13) assume that the same forces that
are active in condensation also produce the phenomenon of
physical (van der Waals) adsorption. This is the basic
assumption of the theory of multimolecular adsorption from
which they derived the following isotherm equation for adsorp-
tion on a free surface:

$$\frac{p}{v(p_o - p)} = \frac{1}{v_m C} + \frac{C - 1}{v_m C} \frac{p}{p_o} \qquad (9)$$

where p is the pressure of the vapor, p_o is the saturation
pressure of the vapor, v is the volume of the vapor adsorbed
at pressure p, v_m is the volume of the vapor adsorbed when the
entire adsorbent surface is covered with a complete mono-
molecular layer, and C is given by the following equation

$$C = e^{E_1 - E_L/RT} \qquad (10)$$

where E_1 is the average heat of adsorption in the first layer
and E_L is the heat of liquefaction. Expressing the amount of

the vapor adsorbed in terms of mass, equation 9 can be made
to read:

$$\frac{p}{q(p_0 - p)} = \frac{1}{q_m C} + \frac{C - 1}{q_m C} \frac{p}{p_0} \tag{9a}$$

where q is the mass of the vapor adsorbed at pressure p, and
q_m is the mass of the vapor adsorbed when the entire adsorbent
surface is covered with a complete monomolecular layer.
Brunauer and his colleagues, considering the factors which
can limit the maximum number of layers that can be adsorbed,
derived a general isotherm equation which shows a perfect fit
with the experimental data and reduces to equations 9 or 9a
at low pressure range (10, 12). Thus, according to BET theory
(theory of multimolecular adsorption) physical adsorption in
the low pressure range is characterized by two parameters
appearing in equations 9 or 9a, namely v_m or q_m and C. Numer-
ical values of these constants can be obtained by making a
straight-line plot of $p/q(p_0-p)$ vs. p/p_0 from experimental
data.

If the area, s, covered by one molecule of the adsorbate
is known, the surface, Σ, of the adsorbent can be calculated
from the value of the parameter v_m or q_m as follows (20)

$$\Sigma = \frac{N v_m s \rho}{M} = \frac{N q_m s}{M} \tag{11}$$

where N is the Avogadro constant, M is the molecular weight
of the adsorbate, and ρ is the vapor density. If, as cus-
tomarily done for convenience, v and v_m or q and q_m are

expressed for one gram of the adsorbent, Σ becomes the specific surface. Emmett and Brunauer (21), assuming closest packing, give the following equation for the area covered by one molecule

$$s = (4)(0.866) \left(\frac{M}{4 \sqrt{2} \, N \delta} \right)^{2/3} = 1.091 \left(\frac{M}{N \delta} \right)^{2/3} \qquad (12)$$

where δ is the density of solidified or liquefied adsorbate, and all other terms have the same meaning as in equation 11. The coefficient 1.091 is designated the packing factor; according to Livingston its value for an adsorbate can vary from one adsorbent surface to another (20, 39, 40). A cross-sectional area of 10.8Å^2 per molecule has been generally accepted for water when the packing factor equals 1.091 (40). Equation 11 can be used either for determining the specific surface area of the adsorbent if the adsorbate cross-sectional area is known with certainty, or for determining the adsorbate cross-sectional area if the specific surface of the adsorbent is known. Using nitrogen as the adsorbate, Emmett et al. found that the specific surface of montmorillonitic clay materials ranged between 41 and 71 m^2/gm (22), whereas using Hendricks et al.'s water adsorption isotherm data (32), Brunauer (10) estimated a specific surface of 400 m^2/gm for montmorillonitic clays. Zettlemoyer et al. (61) from ammonia adsorption isotherms of sodium montmorillonite obtained a specific surface of 556 m^2/gm, but their water adsorption

isotherm data did not produce a linear BET plot. All these
areas are based on closest packing of the adsorbate on the
adsorbent surface. The large difference between the specific
surfaces obtained by nitrogen and water or ammonia was thought
to be due to the penetrability of the adsorbates; water or
ammonia being able to penetrate between the layers of mont-
morillonite, while nitrogen merely covers the external sur-
faces of the organized particles (10, 49, 61). However, the
specific surface obtained from water or ammonia adsorption
isotherms is only about 1/2 to 2/3 of the specific surface
calculable from crystallographic data (10, 30, 61). Mooney
et al. (49) by using water desorption isotherms (which, how-
ever, started below saturation) for sodium and hydrogen mont-
morillonite have obtained specific surfaces in agreement with
crystallographic data. In another study, however, they could
not reproduce these results (50).

Other investigators, emphasizing the ice structure or
the formation of hydrogen bonds between water molecules and
oxygens of the surface layer of clay minerals, suggested
relatively loose arrangements of water molecules on clay
mineral surfaces (5, 31, 32, 41). Loose packing has been
evidenced by rather recent investigations (1, 7, 16) of the
density of the hydrated mineral, which indicate that the
density of the adsorbed water is less than 1. Some of the
earlier investigations indicated density values larger than 1

as well as lower than 1 (30, p. 171). Variations in density values arise from the experimental difficulties from bulk density measurements (16).

In the BET equation, parameter C, which can be evaluated from the straight line plot of equation 9a, includes the average heat of adsorption, E_1, for the first layer (equation 10). Calculated values for the average heat of adsorption for the first layer from these relationships are less than measured average heats of adsorption, but they are of the right order of magnitude (11). Clampitt and German (14) have shown that the heats of vaporization of thin films of a liquid are different from the heat of vaporization of the bulk liquid, and are calculable from the film thickness. By assuming that the heat of vaporization for second and higher adsorbed layers varies depending on the film thickness instead of being constant and equal to the heat of vaporization of the bulk liquid as assumed in the original BET theory, they re-derived the two parameter BET equation. This treatment did not change the form of the BET equation; it only changed the meaning of C. According to the Clampitt and German treatment the exponential term in C contains $E_1 - E_L + (\Delta H_S - E_L)$ instead of only $E_1 - E_L$. The correction term $(\Delta H_S - E_L)$, where ΔH_S is the heat of vaporization of the surface layer, accounts for the difference in the heat of vaporization of successive layers. The value for various adsorbates has been calculated by these

investigators (14), who by applying this correction obtained much better agreement between the values of $E_1 - E_L$ determined from adsorption isotherms and from heat of emersion experiments (11). $E_1 - E_L$ values reported in the present study have been corrected according to Clampitt and German, using their correction value of $(\Delta H_S - E_L) = 1700$ cal/mol for water.
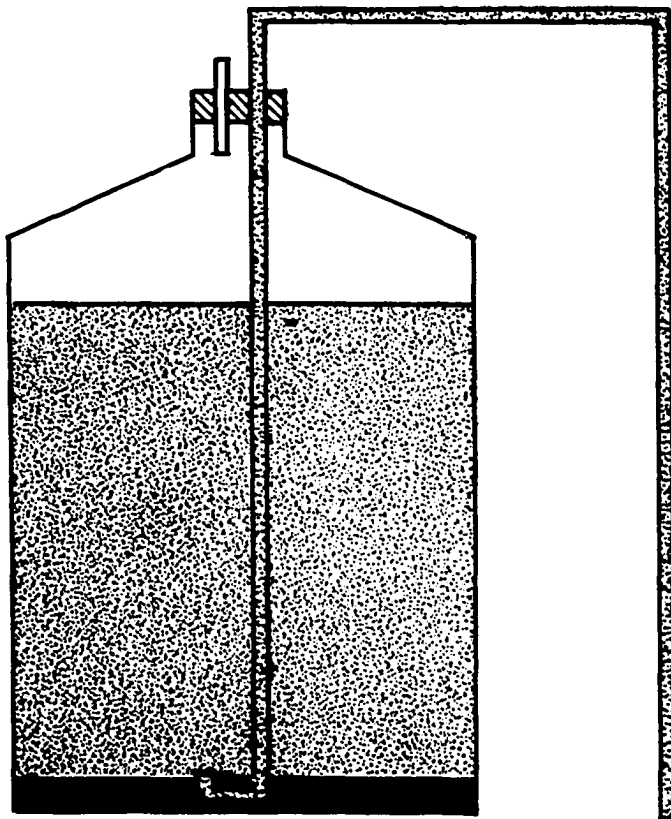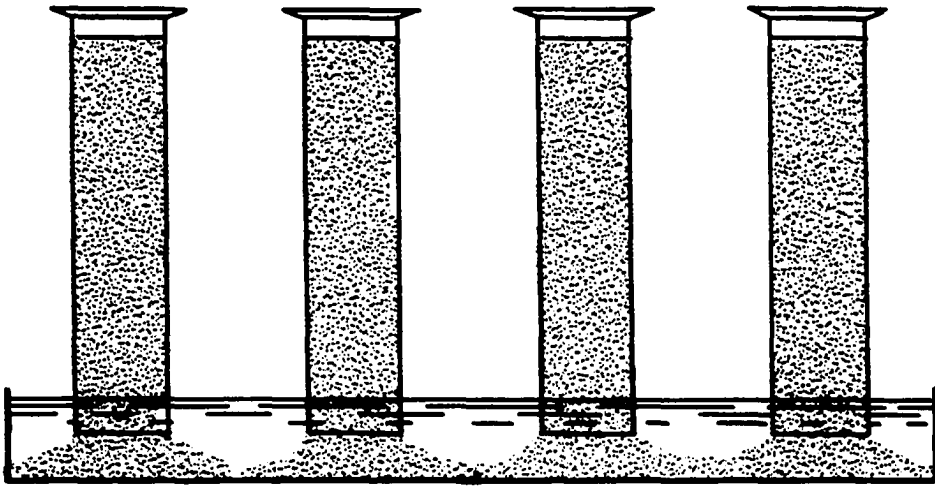
MATERIALS

Montmorillonite

The montmorillonite used was a commercially available Wyoming bentonite known by the trade name Volclay-SPV and produced by American Colloid Company. According to the producer it consists of 90 percent montmorillonite which is essentially a sodium montmorillonite, and 10 percent other minerals, mainly felspar, quartz and volcanic glass. The Volclay-SPV sample was purified by sedimentation: It was first dispersed in distilled water by mixing for 24 hours with a motor stirrer to produce a suspension at a concentration of 60 grams per liter. After dispersion, the suspension was transferred into one-liter cylinders which were shaken end-to-end and inverted and dipped into a shallow pan containing distilled water. The height of the suspension in the cylinders was 40 centimeters (Figure 2). The cylinders were kept in this position for 48 hours to settle out the coarse particles, after which the suspension was placed into a carboy and diluted with distilled water to double its volume. The height of the suspension in the carboy was 30 centimeters. The carboy then was shaken end-to-end for a period of ten minutes and left for sedimentation for four days. At the end of this period the supernatant suspension was separated from the sediment by syphoning into another carboy with a U-shaped tube as illus-

Figure 2. Inverted cylinder arrangement for the separation
of coarse particles from suspension

Figure 3. Syphon arrangement for the separation of suspension
from sediment

trated in Figure 3. The removed suspension was again shaken
end-to-end for ten minutes and left for sedimentation for four
days. This procedure was repeated twelve times, until the
suspended material was practically freed from impurities.
Samples taken from the residue and from the suspended material
were checked by X-ray diffraction for impurities; an X-ray
pattern from the dried suspension sample after the last sedi-
mentation is shown in Figure 4. The concentration of the sus-
pension thus obtained was 20 grams per liter as determined by
evaporating the liquid from a known volume of the suspension;
the cation exchange capacity of the suspended montmorillonite
was found to be 98 milli-equivalents per 100 grams. This sus-
pension was used in the preparation of sodium and calcium
montmorillonites.

To prepare sodium montmorillonite 500 cubic centimeters
of saturated sodium chloride solution (550 milli-equivalents
of sodium ions per 100 cubic centimeters) prepared from re-
agent grade sodium chloride and distilled water, was added
slowly into 3.5 liters of the suspension under constant
vigorous stirring. The amount of the sodium ions thus added
was about 40 times that needed to satisfy the cation exchange
of the montmorillonite present in the suspension. The mixture
was stirred with a motor stirrer for 24 hours to attain equi-
librium for ion exchange. At the end of this period, to sep-
arate the clay from the solution the mixture was centrifuged

Figure 4. X-ray diffraction chart of purified Volclay-SPV
obtained by using filtered chromium radiation

Purified Volclay SPV

2θ, degrees

d, Å
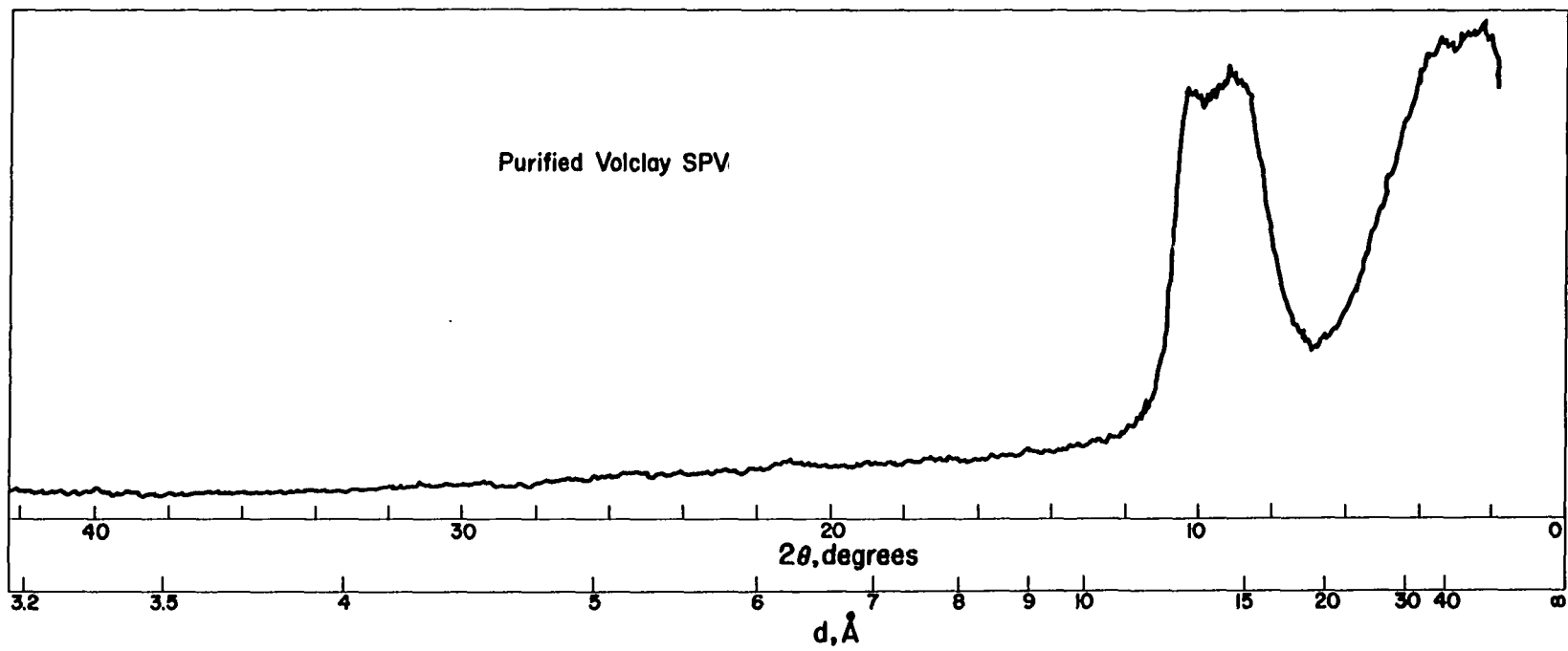
using a motor driven, open type Sharples supercentrifuge
(Model T-1) equipped with a standard clarifier rotor (No.
1-H). With this centrifuge it was possible to obtain an
acceleration of 13,200 g. This acceleration with a feed rate
of 15 cubic centimeters per minute made possible separation
of all clay particles larger than 0.03 micron nominal diam-
eter. The clay material thus separated, after being re-
dispersed in 3 liters of distilled water, was treated with
200 cubic centimeters saturated sodium chloride solution,
stirred for 24 hours and centrifuged again as described above.
This process was repeated five times in total to assure re-
placement of all other cations associated with the mont-
morillonite sample by sodium ions. Next the sample was washed
to free it from the free electrolyte by redispersing it in
distilled water, stirring for 24 hours, and centrifuging.
The washing process was repeated four times till the centri-
fugate tested out free of chloride ions. All centrifugates
were clear and practically free of suspended particles. The
centrifuged sample was dried in an oven kept at 40° C for
several weeks. Then it was ground with a mortar and pestle
to pass through a 140 mesh U.S. standard sieve.

The calcium montmorillonite sample was prepared by using
the same procedure used for sodium montmorillonite except
that less saturated calcium chloride solution (1100 milli-
equivalents of calcium ions per 100 cubic centimeters) was

used for ion exchange. In each of the five steps of extraction, 100 cubic centimeters of saturated calcium chloride solution was used instead of 500, 200, 200, 200 and 200 cubic centimeters used for preparing sodium montmorillonite. The amount of the calcium ions thus added was about 16 times as much as that needed to satisfy the cation exchange of the montmorillonite present in the suspension.

X-ray diffraction analyses performed on the samples thus prepared, showed that they were pure calcium and sodium montmorillonites (Figures 11 and 12). The physical and chemical properties were determined following standard procedures. These properties are listed in Table 1.

Distilled Water

The distilled water used for the preparation of the samples was obtained from a steam-operated SLH-2 Barnstead still which produces, when fresh, practically carbon dioxide free distilled water with a pH approaching 7. To be used in adsorption experiments, this distilled water after running through an exchange column was triple distilled and boiled vigorously just before introducing into the adsorption apparatus.

Sodium Chloride

The sodium chloride used was reagent grade chemical meeting A.C.S. specifications.

Table 1. Properties of the minerals used

Mineral	Sodium montmorillonite	Calcium montmorillonite
Physical properties		
Liquid limit, %[a]	968	341
Plastic limit, %[b]	51	46
Plasticity index, %	917	295
Shrinkage limit, %[c]	17	34
Centrifuge moisture equivalent, %[d]	882	173
Chemical properties		
Cation exchange capacity, m.e/100 gm[e]	94	103
pH[f]	7.55	6.60

[a]ASTM Method D423-54T.

[b]ASTM Method D424-54T.

[c]ASTM Method D427-61.

[d]ASTM Method D425-39.

[e]Ammonium acetate method.

[f]Glass electrode method using suspension of 1 gm soil in 30 cc distilled water.

Calcium Chloride

The calcium chloride used was reagent grade calcium chloride dihydrate meeting A.C.S. specifications.

Mercury

Mercury used in the diffusion pump and manometers was C.P. grade triple distilled mercury.

METHODS OF INVESTIGATION

The adsorption isotherms were determined by using the gravimetric method (10). The X-ray diffraction method (8) was used for studying the interlayer spacings at various relative pressures of water vapor.

Apparatus

The adsorption apparatus used was a McBain-Bakr (47) quartz spring balance connected to a vacuum train by means of a large mercury-sealed stopcock, and immersed in a water thermostat at 24.34° C (Figure 5). The vacuum train consisted of a rotary single stage forepump (Cenco-Hyvac), a single stage mercury diffusion pump, a cold trap containing liquid nitrogen, and a McLeod gauge. The thermostat was made of plexiglass fitted with optical glass observation windows and equipped with a continuous heater, a tap water cooling coil, a motor stirrer, a Beckman thermometer reading to 0.01° C, and an intermittent heater-mercury regulator-relay circuit. The heaters were two 110 volt, 100 watt, light bulbs, the voltage being controlled by means of variable transformers to obtain the best temperature control. The room was air-conditioned and its temperature was maintained at about 3° C above the thermostat temperature to avoid condensation on parts exposed to the air. The variation in the thermostat temperature was not more than $\pm 0.02^\circ$ C throughout
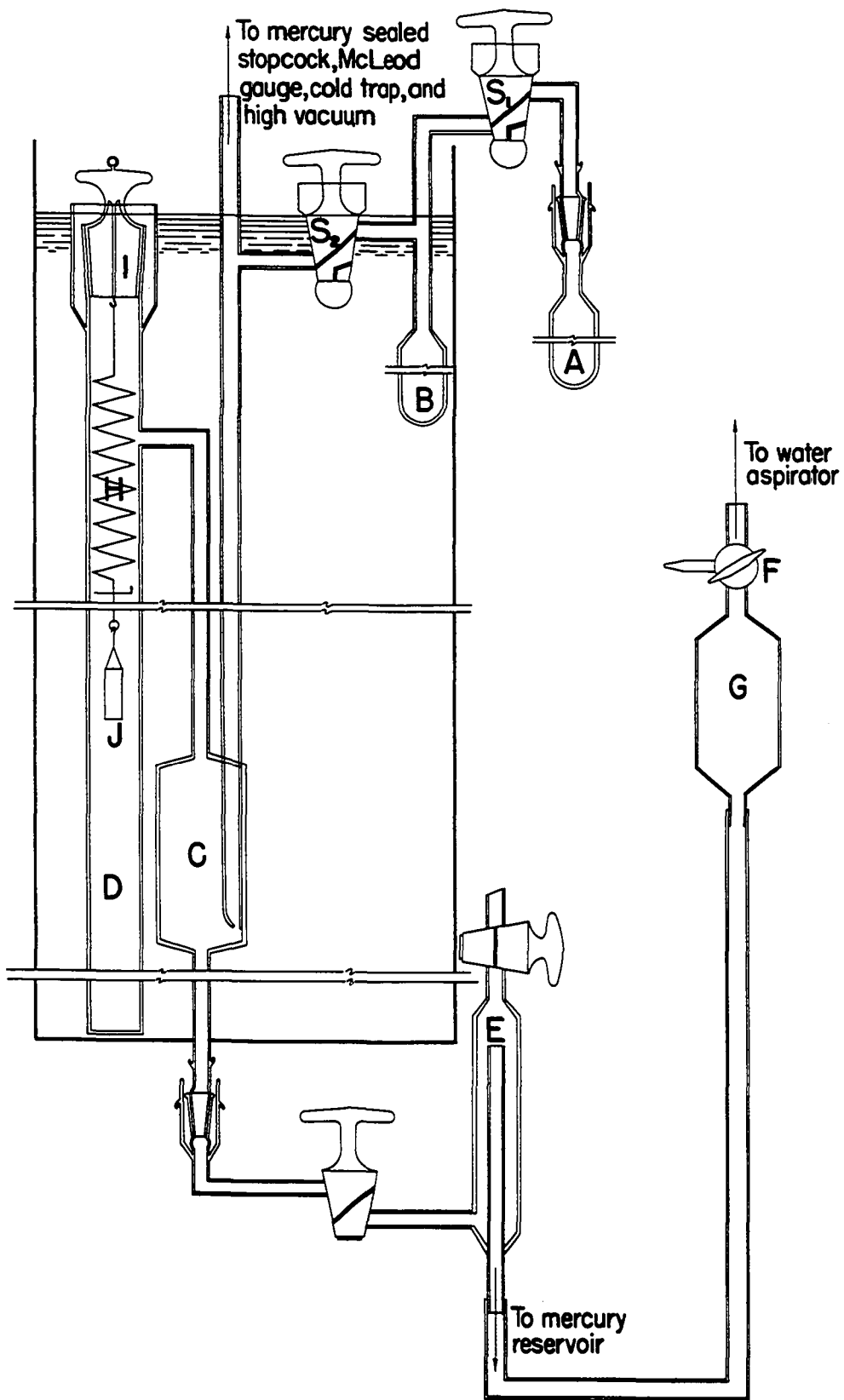
Figure 5. Equipment for adsorption measurements
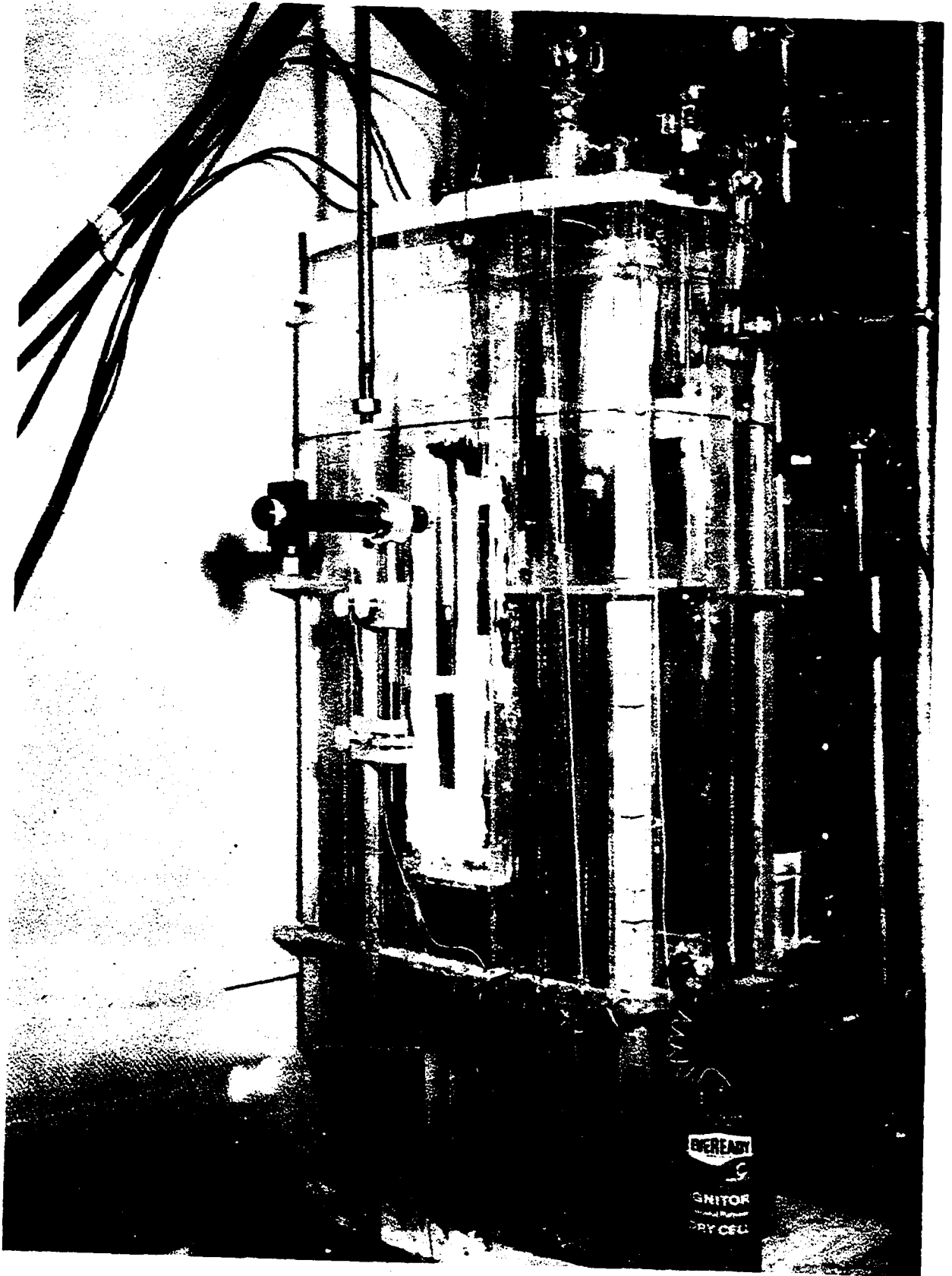
the entire testing period and ± 0.002° C when readings were taken. The Beckman thermometer was calibrated against a N.B.S. certified thermometer at the thermostat temperature.

The adsorption apparatus is shown in Figure 6. The bulb A attached to the system by means of a mercury-sealed joint is the water reservoir for introducing water into the system. The bulb B is the permanent water reservoir into which water is transferred from the bulb A by distillation under high vacuum. C is a simple mercury manostat-manometer combination for transferring water vapor into the adsorption chamber D and for measuring the vapor pressure. The mercury in C can be raised and lowered through the air trap E by means of the two way stopcock F joining the mercury reservoir G to a water aspirator. All the glass parts are Pyrex. High vacuum silicone grease was used for all joints. The quartz spring balance* H is suspended in the adsorption chamber by means of a hook attached to the mercury-sealed ground-glass stopper I. The load capacity of the balance is 2 grams, and the balance extension at this load is 20 centimeters. The balance sensitivity was found to be 0.103, 0.102 and 0.101 millimeters per milligram with 0.12, 0.50 and 1.00 gram balance loads respectively, which is in exact agreement with the manufacturer's data. Suspended from the hangdown loop of the spring balance is the sample holder J. The sample holders were made

---

*Obtained from Microchemical Specialties Co., Berkeley, California.

Figure 6. Adsorption apparatus

To mercury sealed
stopcock, McLeod
gauge, cold trap, and
high vacuum

S_1

S_2

A

B

To water
aspirator

F

G

I

H

J

C

D

E

To mercury
reservoir

from thin wall glass tubing and weighed less than 0.3 gram.

The spring balance extensions were determined through the optical glass observation window of the thermostat by using an optical reader[*] which was calibrated by the manufacturer using a stage micrometer. The optical reader has a 5 millimeter objective field divided into 1000 divisions by means of a filar micrometer eyepiece containing a movable crossline. As certified by the manufacturer 398.9 ± 0.1 divisions of the filar micrometer are equivalent to 2.0000 ± 0.00005 millimeters. The length of one division calculated from this information is 0.005013 ± 0.000002 millimeters (57, p. 20).

A cathetometer reading to 0.02 mm was used for measuring the levels of the mercury in the manometer C through the optical glass observation window.

To prevent differential movements the adsorption apparatus, the optical reader and the cathetometer were securely mounted on a rigid steel frame tied to a heavy soapstone table top and a concrete base.

A General Electric XRD-5 diffractometer with filtered chromium radiation was used in the X-ray diffraction study. To maintain the desired relative humidity during the run a plexiglass hood containing a desiccant or a saturated solution

---

[*]Obtained from Microchemical Specialties Co., Berkeley, California.

giving the desired humidity and provided with a Mylar window
for the free passage of X-rays was placed over the sample.

Preliminaries

Spring balance calibration

The spring balance was recalibrated with the optical
reader with analytical balance weights which were first
checked and calibrated on a certified analytical chain bal-
ance. From these data the calibration chart given in Figure
7 was constructed to evaluate the weight of the vapor adsorbed
from spring extension.

Buoyancy correction to the spring balance

The balance extension due to evacuation from 738 milli-
meters Hg air pressure down to 10^{-5} millimeters Hg was deter-
mined by taking spring balance readings before and after
evacuation. The extension corresponded to 0.15 milligrams.
The buoyancy volume of the spring was calculated from this
value as follows, by assuming ideal gas behaviour and an
average molecular weight of 29 for air:

$$V = \frac{m_a \, RT}{M_a \, p} = \frac{0.00015 \times 62361 \times 298}{29 \times 738}$$

By assuming ideal gas behaviour for water vapor, the buoyancy
correction for 1 millimeter water vapor pressure was calcu-
lated as follows:

Figure 7.   Spring balance calibration chart

Figure 8.   Capillary depression of the apex of a mercurial
column in a glass tube 6 millimeters in diameter
vs. meniscus height

Balance
sensitivity,
s, mg/div

Balance load, W, grams

Depression
of the apex,
mm

Meniscus height, mm
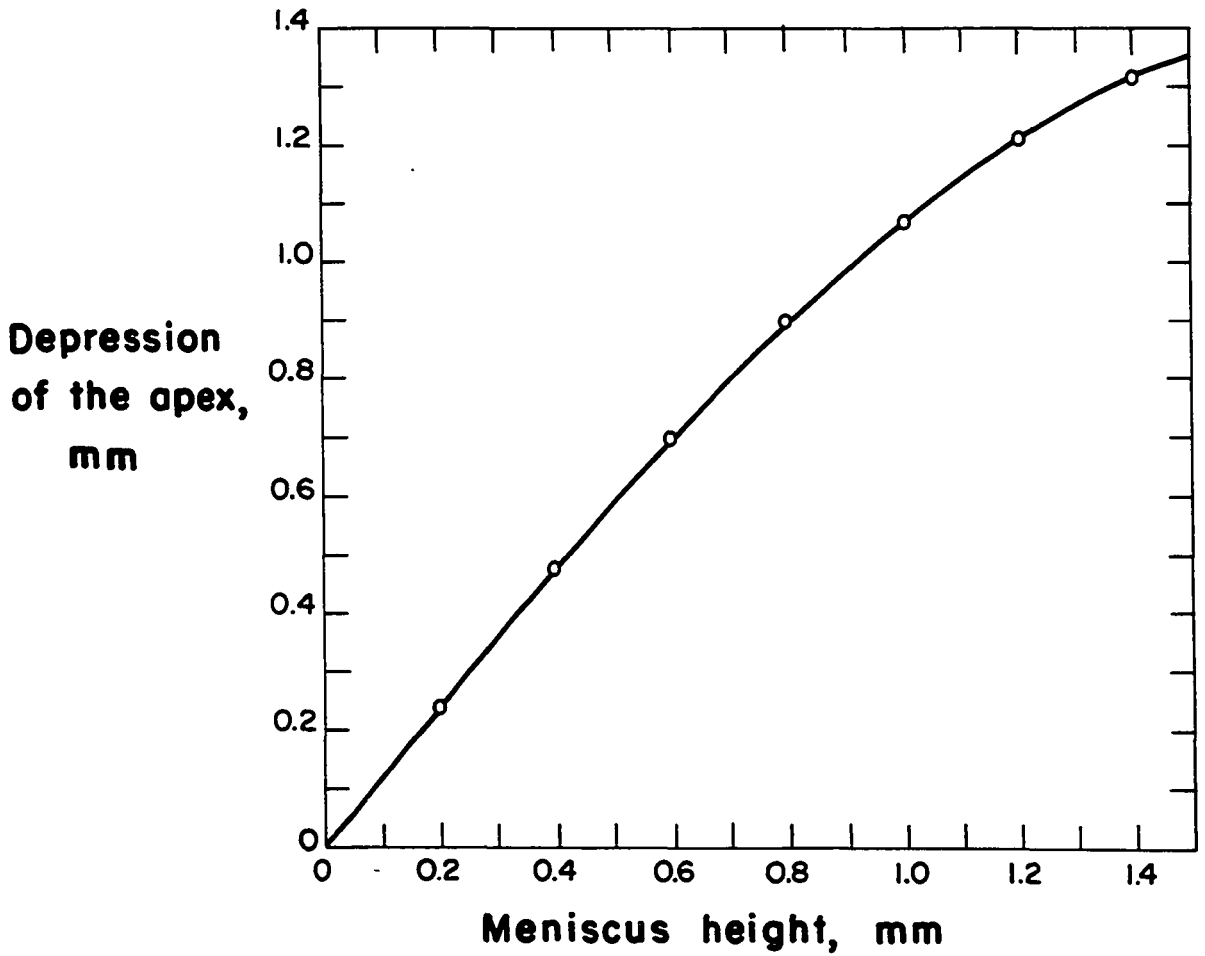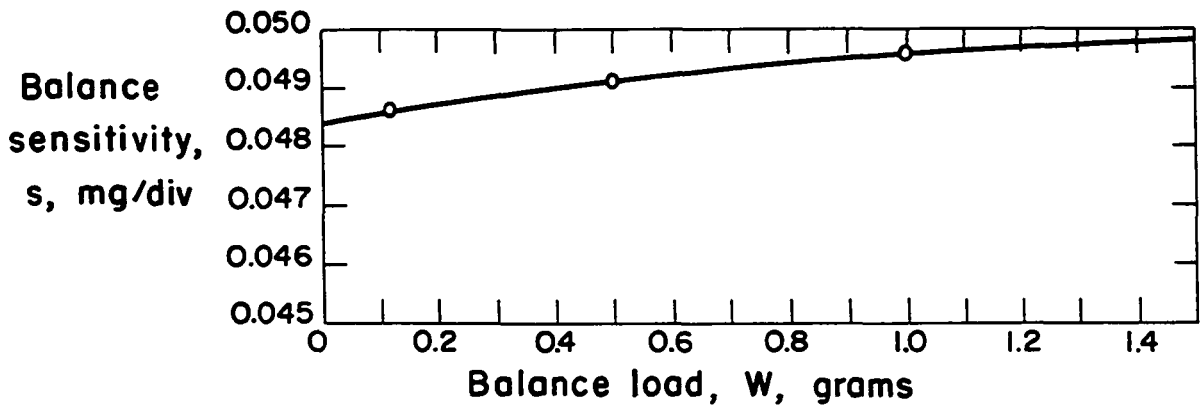
$$m_w = V \frac{M_w \; p}{RT} = \frac{0.5}{2.5} \; \frac{18 \times 1}{62361 \times 298} = 0.0001_3 \; mg/mm$$

The buoyancy correction due to the sample and sample holder was calculated as follows, assuming an average density of 2.5 grams per cubic centimeter and an average total weight of 0.5 grams:

$$m_w = V \frac{M_w \; p}{RT} = \frac{0.5}{2.5} \; \frac{18 \times 1}{62361 \times 298} = 0.0001_9 \; mg/mm$$

The total buoyancy correction was 0.0003_2 milligrams per millimeter Hg of water vapor. Since this correction was insignificant for most of the adsorption isotherms and within the experimental errors for the remainder, no further refinement was made.

Meniscus correction to mercury levels in the manometer

The mercury levels in each arm of the manometer were corrected for capillary depression of the apex of the mercurial column, since meniscus heights were found to differ slightly due to difference in water vapor pressures in the two arms. Using the data obtained from International Critical Tables (51) Figure 8 was constructed. For each mercury level the meniscus height was determined, and the level reading was corrected by adding to it the depression of the apex obtained from Figure 8.

Gravity and temperature correction to mercury manometer

The vapor pressure readings obtained were converted to the standard scale as follows:

$$h_o = \frac{dg}{d_o g_o} h$$

where h_o is the corrected manometer reading, d and d_o are the densities of mercury at thermostat temperature (24.34^o C) and at 0° C, respectively, g and g_o are local and standard acceleration of gravity, respectively, and h is the observed manometer reading. Values d_o = 13.5951 gm/cc, d = 13.5356 gm/cc and g_o = 980.665 cm/sec^2 were obtained from the literature (33). The local value for acceleration of gravity is g = 980.297 cm/sec^2.[*] Substituting these values into the equation given above the following relationship was obtained between the observed and correct manometer readings:

$$h_o = 0.9952 \ h$$

The vapor pressures observed were corrected by using this relationship.

Procedure

Determination of the adsorption isotherms

The calcium and sodium montmorillonite samples were

---

[*]S. Legvold, Professor of Physics, Iowa State University of Science and Technology, Ames, Iowa. Personal communication. 1962.

introduced into the sample holders by pouring through small glass funnels. The samples were packed by tapping and placed in ground glass stoppered weighing bottles. The weighing bottles with stoppers kept open were then placed in a vacuum desiccator containing phosphorous pentoxide, and the desiccator evacuated and the samples left in it to dry for several weeks. After the drying process the vacuum was released through a moisture trap containing phosphorous pentoxide, and the weighing bottles were immediately stoppered and weighed. The calcium montmorillonite sample was returned to the desiccator and the desiccator was evacuated. The sodium montmorillonite sample was introduced into the adsorption apparatus by hanging on the hangdown loop of the spring balance which had been previously suspended by a string and pulley arrangement above the adsorption chamber. The balance and the sample were then lowered into the adsorption chamber and the stopper (I, Figure 6) was sealed with mercury. Water was introduced into the bulb A and frozen by dipping the bulb in liquid nitrogen contained in a dewar flask. Then the adsorption apparatus was pumped down to 10^{-5} millimeters. After the attainment of high vacuum, mercury was raised in manometer C to cut off the adsorption chamber from the rest of the apparatus. The stop-cock S_1 connecting bulb A to the adsorption apparatus was turned off, the water was melted to release the dissolved gases, re-frozen, and the apparatus pumped

again. This process of degassing the water was repeated five times, after which the stopcock S_2 was closed and the water was redistilled into the permanent water reservoir B by dipping the reservoir in liquid nitrogen contained in a dewar flask suspended in the thermostat and raised about the reservoir by a string and pulley arrangement. After distillation, stopcock S_2 was opened and the water reservoirs were pumped once more. Then both of the stopcocks, S_1 and S_2, were turned off. The mercury in manometer C was lowered and the sample was pumped down to 10^{-5} millimeters for several days for degassing. During degassing as much of the apparatus as possible was heated with a hand torch; the sample was not heated because of the heat sensitivity of clays. After degassing, the mercury was raised in manometer C, the mercury-sealed main stopcock connecting the adsorption apparatus to the vacuum train was turned off, and water vapor was introduced into the right hand limb of the manometer by opening the water reservoir stopcock, S_2. This stopcock was held open for the rest of the experiment. The thermostat was filled with water and brought to 24.34° C.

After the attainment of thermal equilibrium with the left limb of the manometer exposed to vacuum and the right exposed to saturated water vapor, a manometer reading was taken. After the usual corrections described above this value agreed with the vapor pressure data given in the literature (33).

After taking the spring balance reading under vacuum the mercury in manometer C was gradually lowered and some vapor was let into the adsorption chamber through the manostat arrangement of the manometer. Then the mercury was gradually raised into the manometer limbs. Particular attention was paid not to compress the vapor to an extent which could affect the adsorption equilibrium. For this purpose a constant or slightly decreasing adsorption rate was maintained by taking continual spring balance readings and adjusting the rate of compression when necessary. The water reservoir was cooled slightly by jacketing it with the dewar flask containing cool water, to prevent condensation in the right limb of the manometer during compression. After the mercury was brought to the proper level a period of 24 hours was found quite sufficient for the attainment of equilibrium. At the end of this period the pressure difference on the manometer and the extension on the spring balance were measured. Making the necessary correction on the pressure difference and subtracting it from the saturation pressure, the equilibrium pressure in the adsorption chamber was obtained. Converting the balance extension to mass increase by using the calibration chart given in Figure 7 and adding the buoyancy correction and dividing by the sample weight, the mass of vapor adsorbed by one gram of adsorbent was obtained. In this way by transferring more and more vapor into the adsorption chamber the pressure range

up to saturation was investigated.

In the vicinity of saturation, an additional technique was introduced: after transferring some vapor into the adsorption chamber a small amount of dew was produced on the upper part of the left hand limb of the manometer by pouring a few cubic centimeters of water at 22° C through a pipette, and the time of disappearance of the dew was observed. At pressures before the saturation the dew disappeared rapidly, whereas at saturation the time of disappearance sharply increased from a few minutes to a few hours. The mass of the water vapor adsorbed just before and at saturation differed about 0.1 percent, indicating accuracy.

After completion of the adsorption isotherm the desorption isotherm was obtained by condensing more and more vapor back into the water reservoir, which was cooled with an ice-water mixture contained in the dewar flask and pumped for low relative pressure range.

The same procedure was used for the calcium montmorillonite sample.

The adsorption and desorption isotherms obtained in this manner are shown in Figures 9 and 10.

X-ray diffraction study

One wet and three dry randomly oriented powder samples of sodium and calcium montmorillonite were packed into 1" x 2" x 1/8" bakelite sample holders. The wet samples were

Figure 9. Adsorption and desorption isotherms of sodium
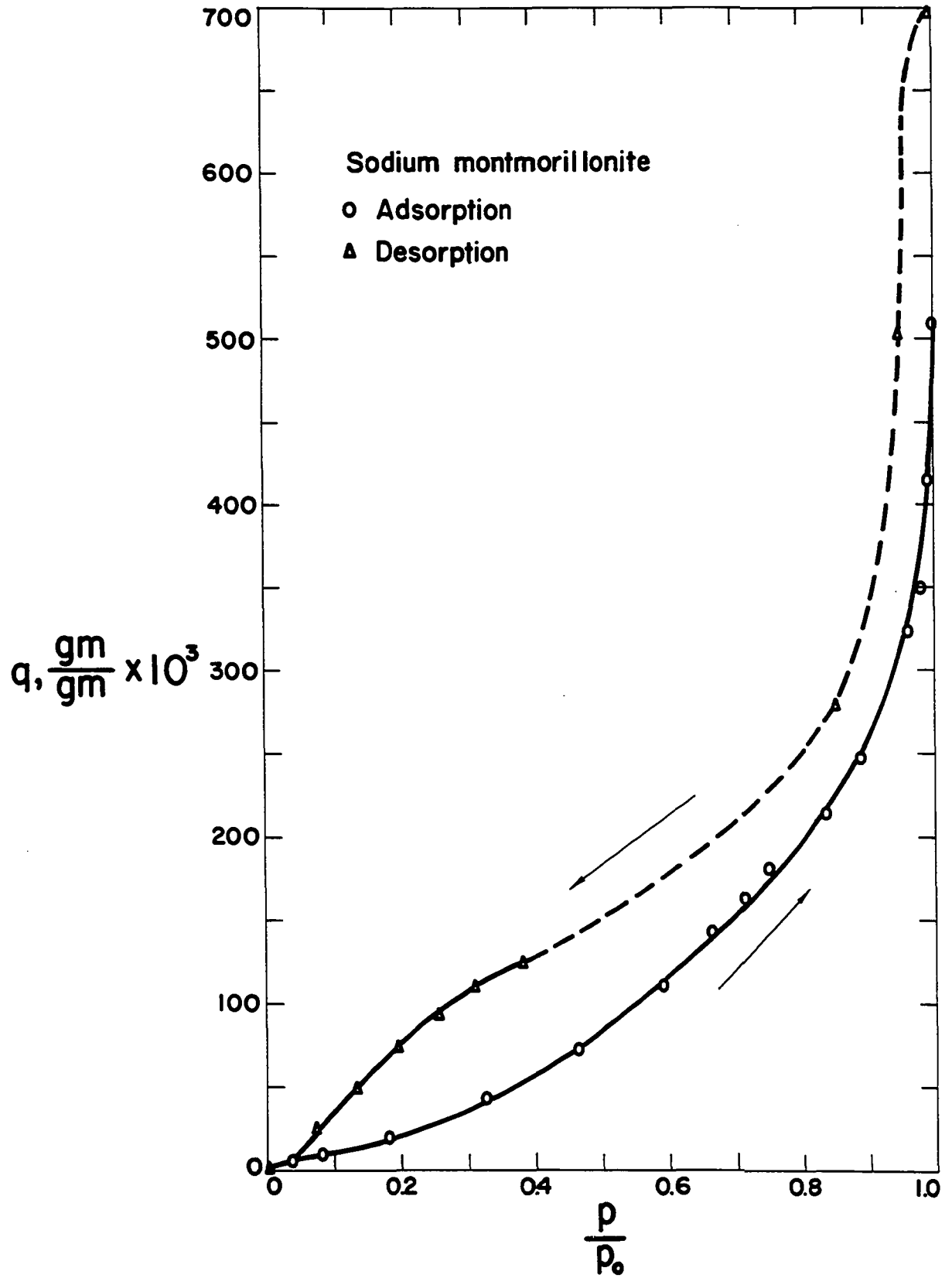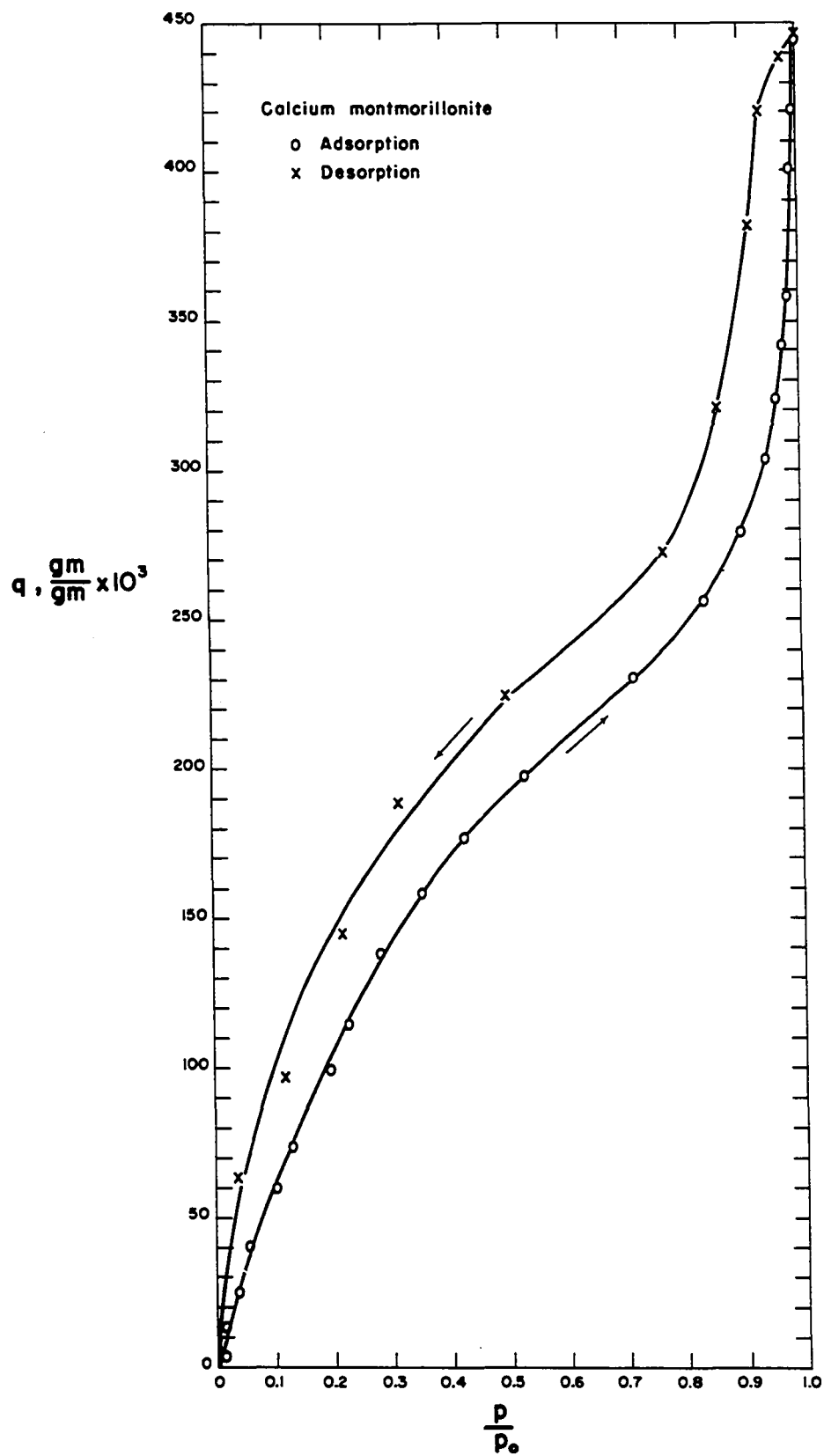montmorillonite

Sodium montmorillonite
o Adsorption
△ Desorption

Figure 10. Adsorption and desorption isotherms of calcium
montmorillonite

Calcium montmorillonite
o   Adsorption
x   Desorption

placed into a humidity chamber maintained at 100 percent relative humidity and the dry samples into vacuum desiccators maintained at 0, 50 and 98 percent relative humidity by means of phosphorous pentoxide, saturated calcium nitrate tetrahydrate solution in equilibrium with the solid phase, and saturated lead nitrate solution in equilibrium with the solid phase, respectively. The desiccators were evacuated and the samples were kept in them for several weeks. After equilibration, samples were taken from the desiccators, mounted on the X-ray diffractometer, covered immediately with the plexiglass hood maintained at the desired relative humidity, and X-rayed.

The X-ray diffraction charts obtained in this manner are shown in Figures 11 and 12.

Errors

Experimental error in determining p/p_o

To test the reproducibility of pressure difference measurement, readings were taken with different amounts of mercury in the manometer with both sides under vacuum. Similar readings were also taken while measuring the vapor pressure of water. The results agreed in each two series of measurements within $\pm$ 0.06 millimeter; $\pm$ 0.04 millimeter of this maximum deviation was due to the cathetometer, and the remaining was apparently due to optical disturbances. The maximum error in the value of p_o due to temperature variations

Figure 11. X-ray diffraction charts of sodium
            montmorillonite at various relative
            humidities

Sodium montmorillonite

Wet sample

$\frac{p}{p_0}=0.98$

$\frac{p}{p_0}=0.50$

$\frac{p}{p_0}=0$
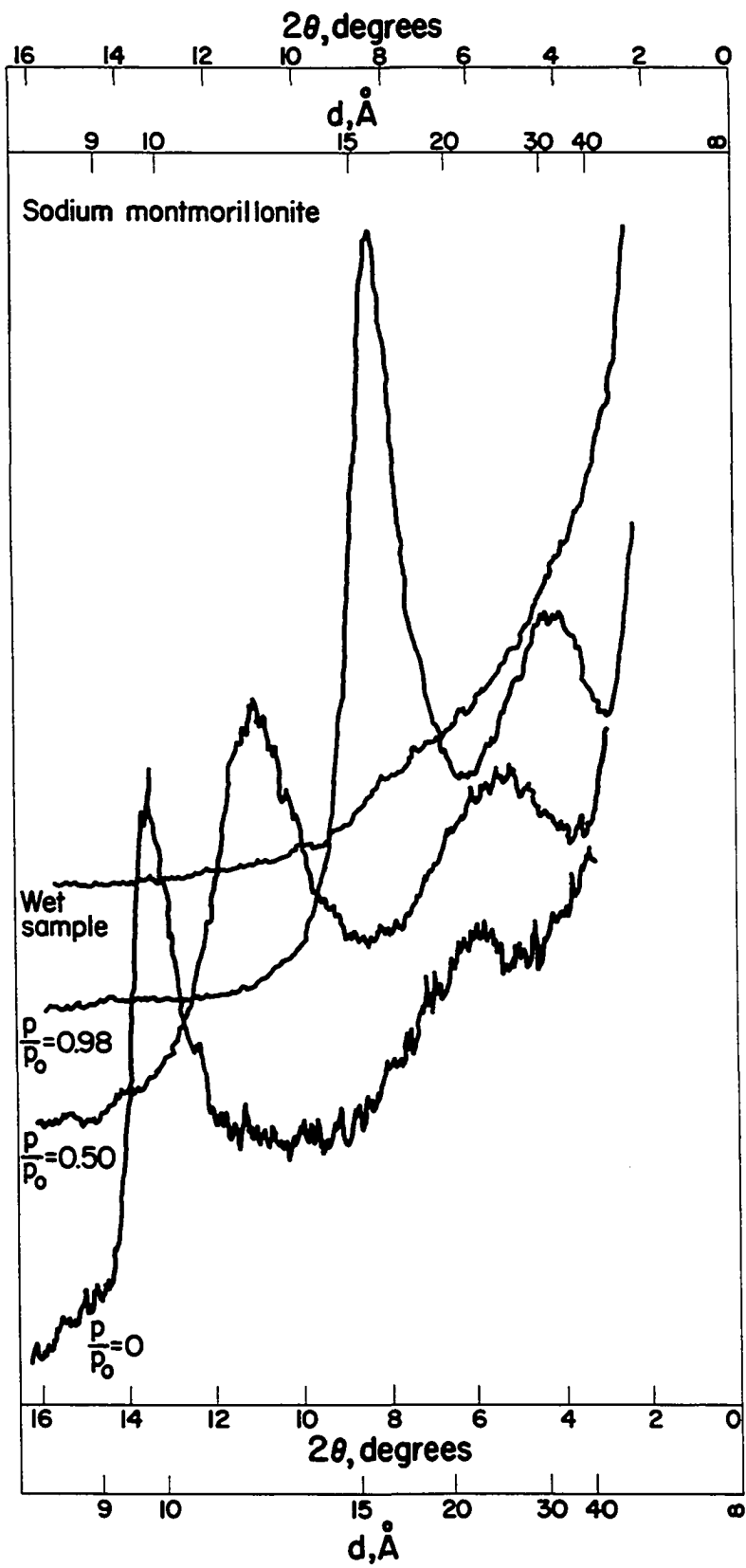
Figure 12. X-ray diffraction charts of calcium montmorillonite at various relative humidities

Calcium montmorillonite

Wet sample

$\frac{p}{p_0}=0.98$

$\frac{p}{p_0}=0.50$

$\frac{p}{p_0}=0$
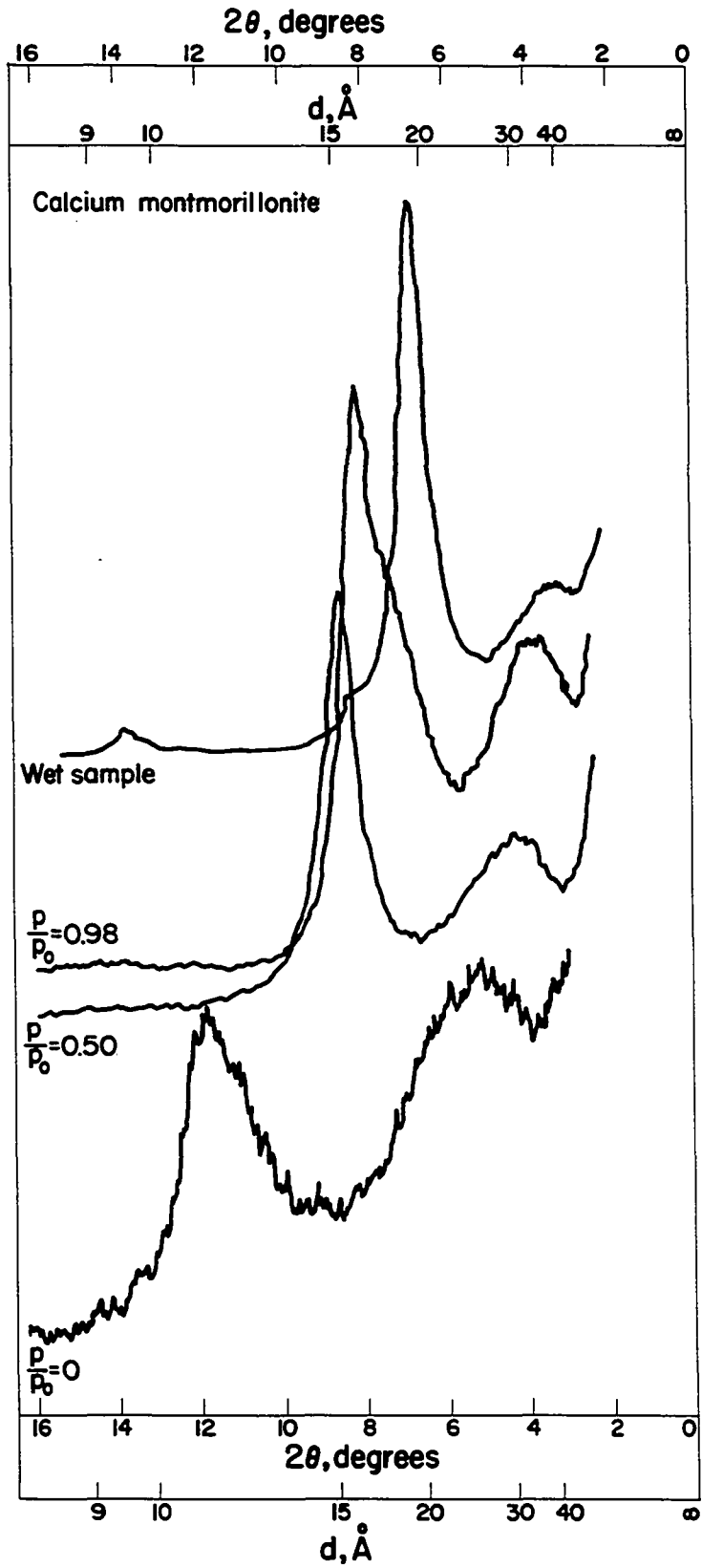
was estimated to be $\pm$ 0.02 millimeters.

The error in p/p_0 was obtained by using the following relationship (57, p. 20):

$$\left(\delta \frac{p}{p_0}\right)^2 = \left(\delta \frac{p_0 - \Delta p}{p_0}\right)^2 = \left(\delta \frac{\Delta p}{p_0}\right)^2$$

$$= \left(\frac{\partial \frac{\Delta p}{p_0}}{\partial \Delta p} \delta \Delta p\right)^2 + \left(\frac{\partial \frac{\Delta p}{p_0}}{\partial p_0} \delta p_0\right)^2$$

which can be expressed:

$$\delta \frac{p}{p_0} = \pm \left[\left(\frac{\delta \Delta p}{p_0}\right)^2 + \left(1 - \frac{p}{p_0}\right)^2 \left(\frac{\delta p_0}{p_0}\right)^2 \right]^{1/2}$$

where $\delta \frac{p}{p_0}$, δp_0 and $\delta \Delta p$ are the errors in $\frac{p}{p_0}$, p_0, and the pressure difference, respectively. The error in $\frac{p}{p_0}$ calculated by this expression was found to be $\pm$ 0.003 for all pressure ranges.

Experimental error in determining q

The weight of adsorbate, q, in grams adsorbed by one gram of adsorbent was calculated by the following equation:

$$q = \frac{l \cdot s}{10^3 w}$$

where l is the spring balance extensions in optical reader divisions, s is the balance sensitivity in milligrams per optical reader division, and w is the sample weight in grams.

The reproducibility of spring balance extension, l, was

tested by taking a series of readings before and after a balance load change. The results were found to agree with each other within $\pm$ 0.2 divisions. The errors in balance sensitivity, s, (Figure 7) and in the sample weight, w, were estimated to be $\pm$ 4 x 10^{-5} and $\pm$ 2 x 10^{-2} milligrams, respectively, from the accuracy of analytical balance used for calibrating the spring balance and weighing the samples. Then the error in q was estimated by using the following relationship:

$$\delta_q = \pm \left[\left(\frac{\partial q}{\partial l}\, \delta_l \right)^2 + \left(\frac{\partial q}{\partial s}\, \delta_s \right)^2 + \left(\frac{\partial q}{\partial w}\, \delta_w \right)^2 \right]^{1/2}$$

from which it follows that

$$\delta_q = \pm \frac{1}{10^3}\frac{s}{w} \left[\left(\frac{\delta_l}{l} \right)^2 + \left(\frac{\delta_s}{s} \right)^2 + \left(\frac{\delta_w}{w} \right)^2 \right]^{1/2}$$

where δ_q, δ_l, δ_s and δ_w are the errors in q, l, s and w, respectively.

The weight, w, of the sodium montmorillonite sample was 0.1866_0 gm and the balance sensitivity obtained from Figure 7 by using total balance load of 0.4871_5 gm (sample and sample holder) was 0.0490_7 mg/division. Substituting these values into the expression given above, the error in q was estimated to be $\pm$ 5 x 10^{-5} gm/gm in the low adsorption range (1 up to 100 division), $\pm$ 2 x 10^{-4} gm/gm in the intermediate adsorption range, and $\pm$ 4 x 10^{-4} gm/gm in the vicinity of complete adsorption.

The error in determining q for the calcium montmoril-
lonite sample was similarly estimated to be $\pm$ 6 x 10^{-5}
gm/gm, $\pm$ 2 x 10^{-4} gm/gm and $\pm$ 4 x 10^{-5} gm/gm in the low and
intermediate adsorption ranges and in the vicinity of complete
adsorption, respectively.

PRESENTATION AND DISCUSSION OF RESULTS

Adsorption Isotherms

Sorption data and the values of the functions for the evaluation of surface area and energy change relationships are presented in Tables 2, 3, and 4,5 for sodium and calcium montmorillonites, respectively.

As may be seen from Figures 9 and 10, adsorption and desorption points fall on two different isotherms, showing hysteresis typical of porous solids (10, 25, 46). On the basis of irreversible hysteresis Mooney et al. assumed that the true equilibrium curve is the desorption branch (49, 50). This is in agreement with the theory offered by Zsigmondy if the irreversibility of hysteresis is persistent in all successive adsorption-desorption runs, and if surface impurities responsible for incomplete wetting are the only cause of the hysteresis (10, p. 394). According to two other theories on the explanation of hysteresis, namely the "ink-bottle" theory of McBain (46) and the "open pore" theory of Foster (25), the adsorption branch is the true equilibrium curve (10, pp. 398, 401). These latter theories explain the hysteresis on the basis of the shape and arrangement of the pores in which capillary condensation takes place. Brunauer states:

> The adsorption process quite often, perhaps always, causes a change in the pore volume. The change caused by the adsorbate is either reversible or irreversible. (10, p. 409).

Table 2. Adsorption isotherm data for sodium montmorillonite

p, mm Hg	p_o, mm Hg	p/p_o	$\frac{gm}{gm}\,{}^{q,}\times 10^3$	$\frac{p}{q(p_o-p)}$	$\frac{q}{p/p_o}$
0.7_9	22.8_4	0.03_5	6.1_8	5.8_0	0.17_9
1.8_8		0.08_2	9.8_7	9.0_9	0.12_0
4.2_1		0.18_4	18.6_8	12.1_0	0.10_1
7.4_6		0.32_7	45.6_4	10.6_3	0.14_0
10.6_4		0.46_6	77.6_4	11.2_3	0.16_6
13.5_5		0.59_3	$110._2$	13.2_3	0.18_6
15.2_0		0.66_5	$144._7$	13.7_4	0.21_7
16.3_6		0.71_6	$163._4$	15.4_5	0.22_8
17.1_5		0.75_1	$182._4$	16.5_2	0.24_3
19.1_4		0.83_8	$214._8$	24.0_7	0.25_6
20.3_0		0.88_9	$248._4$	3_2	0.27_9
22.0_4		0.96_5	$327._1$	8_4	0.33_9
22.4_4		0.98_3	$349._8$		0.35_6
22.7_3		0.99_5	$413._7$		0.41_6
22.8_4		1.00_0	$510._5$		0.51_0

The irreversible change in the pore volume may result in different pore shapes and pore arrangements, and change the intersticial surface areas in case of interacting solids like sodium or calcium montmorillonite, giving rise to an irreversible hysteresis. Essentially similar explanations have been

Table 3. Desorption isotherm data for sodium montmorillonite

p, mm hg	p_0, mm Hg	p/p_0	q, $\frac{gm}{gm} \times 10^3$	$\frac{p}{q(p_0-p)}$
22.8_4	22.8_4	1.00_0	$699._0$	
21.6_5		0.94_8	503.4	
19.3_5		0.84_7	279.3	$19._8$
8.8_0		0.38_5	$124._1$	5.0_5
7.1_9		0.31_5	$109._0$	4.2_1
5.9_2		0.25_9	96.8_1	3.6_1
4.5_1		0.19_7	77.7_1	3.1_7
3.0_2		0.13_2	50.1_3	3.04
1.6_8		0.07_4	22.7_7	3.4_9

given by others for the irreversible hysteresis observed in the case of adsorption of water on ferric oxide gel or on fine powders of calcite (17, 54). These investigators believed that the drift in consecutive adsorption-desorption experiments was due to a growth of the particles. With this explanation each adsorption and desorption experiment corresponds to a different initial and final state, but the adsorption branch remains as the true equilibrium curve for a single adsorption experiment. Since the impurities causing Zsigmondy type hysteresis can be minimized by effective degassing, the pore structure probably remains the main cause of the

Table 4. Adsorption isotherm data for calcium montmorillonite

p, mm Hg	p_0, mm Hg	p/p_0	q, $\frac{gm}{gm} \times 10^3$	$\frac{p}{q(p_0-p)}$	$\frac{q}{p/p_0}$
0.3_0	22.8_4	0.01_3	3.7_7	3.5_3	0.29_0
0.3_9		0.01_7	12.4_5	1.3_9	0.73_2
0.8_1		0.03_5	26.2_0	1.4_0	0.74_9
1.2_9		0.05_6	40.7_9	1.4_7	0.72_2
2.3_4		0.10_2	60.0_1	1.9_0	0.58_8
2.9_9		0.13_1	74.1_9	2.0_3	0.56_6
4.5_0		0.19_7	99.1_1	2.4_8	0.50_3
5.2_4		0.22_9	114.3	2.6_1	0.49_9
6.4_4		0.28_2	$138._5$	2.8_3	0.49_1
8.0_4		0.35_2	$158._9$	3.4_2	0.45_2
9.7_6		0.42_7	$177._1$	4.2_1	0.41_5
12.0_9		0.52_9	$197._6$	5.6_9	0.37_3
16.3_8		0.71_7	$230._1$	11.0_2	0.32_1
19.1_1		0.83_7	$256._6$	19.9_7	0.30_7
20.5_3		0.89_9	$279._3$	3_2	0.31_1
21.5_3		0.94_3	$303._5$	5_4	0.32_2
21.9_6		0.96_1	$323._6$	7_7	0.33_6
22.1_6		0.97_0	$342._1$	9_5	0.35_3
22.4_5		0.98_3	$358._6$		0.36_5
22.5_2		0.98_6	$400._3$		0.40_6
22.6_8		0.99_3	$421._0$		0.42_4
22.8_4		1.00_0	$444._0$		0.44_4

Table 5. Desorption isotherm data for calcium montmorillonite

| p, mm Hg	p_o, mm Hg	p/p_o	q, $\frac{gm}{gm} \times 10^3$	$\frac{p}{q(p_{o_{-1}}-p)}$
22.84	22.84	1.000	446.8	
22.23		0.973	438.5	
21.33		0.934	420.2	33
20.87		0.914	381.3	28
19.64		0.860	320.9	19.1
17.51		0.767	272.2	12.07
11.31		0.495	224.7	4.36
7.12		0.312	188.3	2.41
4.99		0.218	144.4	1.94
2.73		0.119	96.59	1.40
0.79		0.035	63.07	0.57

hysteresis. For these reasons, in this study the adsorption branch was assumed to be the true equilibrium curve.

At saturation pressure, temperature had a curious effect in the experiment with sodium montmorillonite. While maintaining the vapor pressure at or very near saturation, when the thermostat temperature was first gradually raised a few degrees, then lowered to the normal value (24.34° C), the sample first lost weight during heating and then gained weight

during cooling, as expected. However, the gain in the sample
weight during cooling and after the attainment of the normal
temperature did not stop at the original equilibrium value,
but kept increasing until another equilibrium value about 20
percent greater than the original was established. This is
shown in Figure 9 by the jump from the last point correspond-
ing to saturation on the adsorption branch to the first point
corresponding to saturation on the desorption branch. Temp-
erature did not have this effect in the experiment with cal-
cium montmorillonite, the two equilibrium values being prac-
tically equal to each other (Figure 10).

This peculiar behavior manifested by sodium montmoril-
lonite is believed to be due to the nature of the potential
of interaction between the platelets of sodium montmoril-
lonite. The total potential of interaction for sodium mont-
morillonite and calcium montmorillonite platelets is schem-
atically represented in Figure 13, based on the arguments put
forward by Overbeek and Verwey (52, 58). This figure indi-
cates that the apex of the energy barrier for sodium mont-
morillonite platelets (point 1 in Figure 13) is located at a
platelet separation distance considerably shorter than that
of calcium montmorillonite (point 2), and the energy barrier
for calcium montmorillonite. If at saturation vapor pressure
the separation distance for sodium montmorillonite platelets
nearly equals the separation distance corresponding to the

Figure 13.   Schematic representation of repulsion, R,
             attraction, A, and total interaction (dashed
             curves) potentials between sodium montmorillonite
             platelets and between calcium montmorillonite
             platelets (sketched using the arguments of
             Overbeek and Verwey (52, 58))
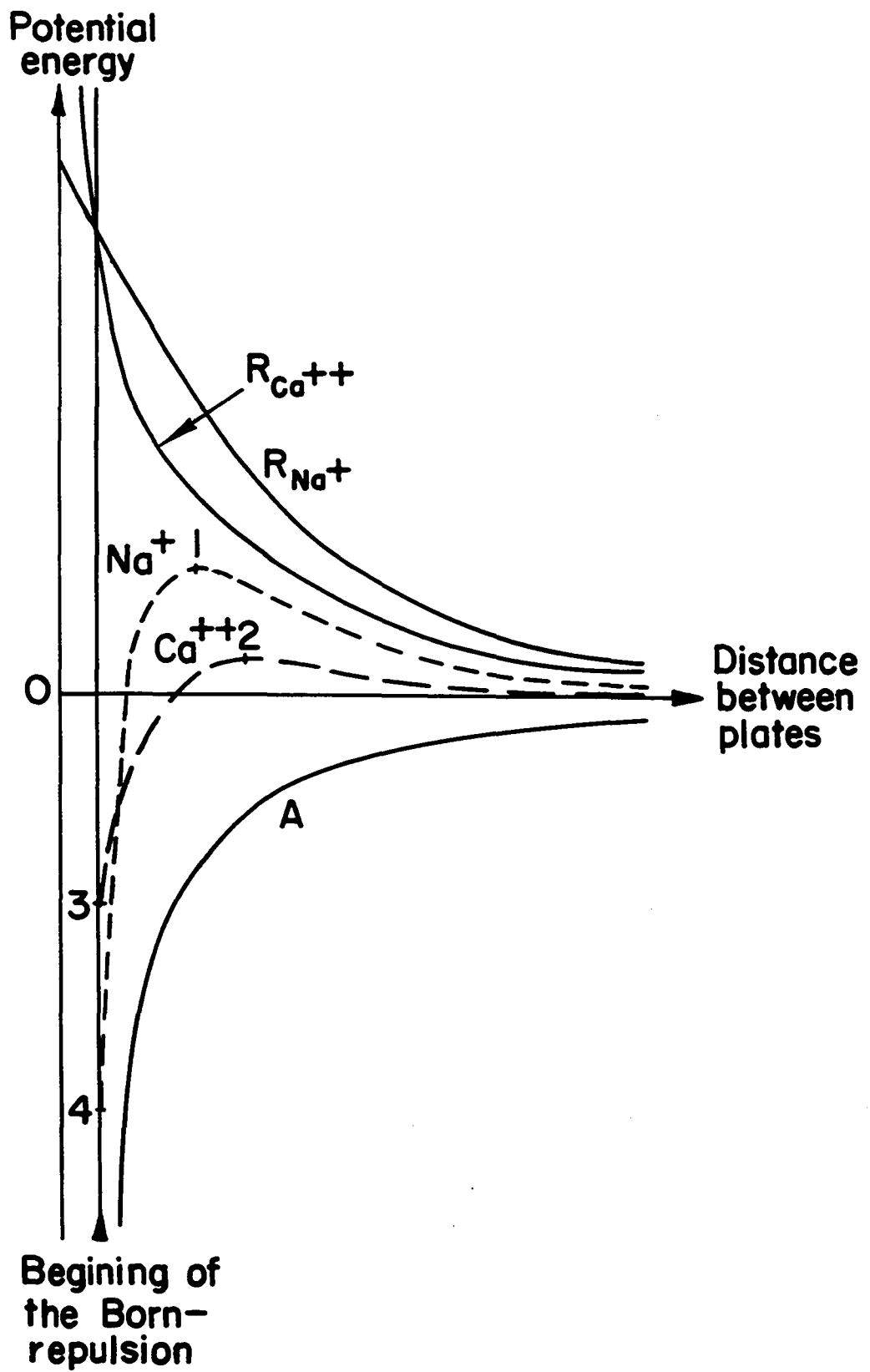
apex of the energy barrier (point 1) the expansion of the
interlayer water due to heating might further separate some
of the platelets past the energy barrier, while total sample
undergoes desorption due to the higher temperature. (For
this to occur it should be assumed that the rate of desorption
is slower than the rate of expansion of the interlayer water
for some of the particles, and the process is actually irre-
versible, the degree of the irreversibility very probably
depending on the rate of heating). The platelets which have
passed the energy barrier will keep adsorbing more and more
water until they attain an equilibrium position. This would
cause further adsorption by sodium montmorillonite already at
equilibrium with saturated vapor, merely by heating a few
degrees and then cooling. This may also explain the expan-
sion and the ease of dispersion of sodium montmorillonite when
directly immersed in water since only a slight temperature
rise, as could be caused by the heat of wetting, may suffice.
Sodium montmorillonite dispersions have been accepted to be
lyophobic colloidal systems, in other words the electrical
double layer is the sole cause of their colloidal stability
(29, 45, 58). However, the argument given above indicates
that solvation of the platelets of sodium montmorillonite may
play an important role on the dispersibility and colloidal
stability of sodium montmorillonite, putting sodium mont-
morillonite somewhere between lyophilic and lyophobic col-

loids.

In the case of calcium montmorillonite the platelet separation distance at saturation vapor pressure may be considerably shorter than the separation distance corresponding to the apex of the energy barrier, and temperature variations can not separate the platelets past the energy barrier apex. Therefore, calcium montmorillonite dispersions would still owe their stability solely to the presence of the electrical double layer, and may be considered as lyophobic colloidal systems.

Figures 9 and 10 were constructed by plotting smooth curves through the experimental points. However, the deviations of the smooth curves from some of the experimental points were found to be more than the experimental errors discussed earlier. The parts of the curves which showed these deviations are reproduced in Figures 14 and 15, together with a new set of curves plotted by directly joining the experimental points. These show a somewhat stepwise trend at 0.15-0.25 relative pressure for calcium montmorillonite and 0.7-0.8 relative pressure for sodium montmorillonite. Although deviations of the smooth curves from experimental points are hardly large enough to really justify a stepwise trend, comparison with X-ray diffraction data (Figure 17) indicates that the relative pressure ranges at which these steps occur nearly equal the relative pressures at which the montmorillonite platelet separations approach the thickness of two

Figure 14. Adsorption isotherm of sodium montmorillonite
            represented by a smooth curve and a stepwise
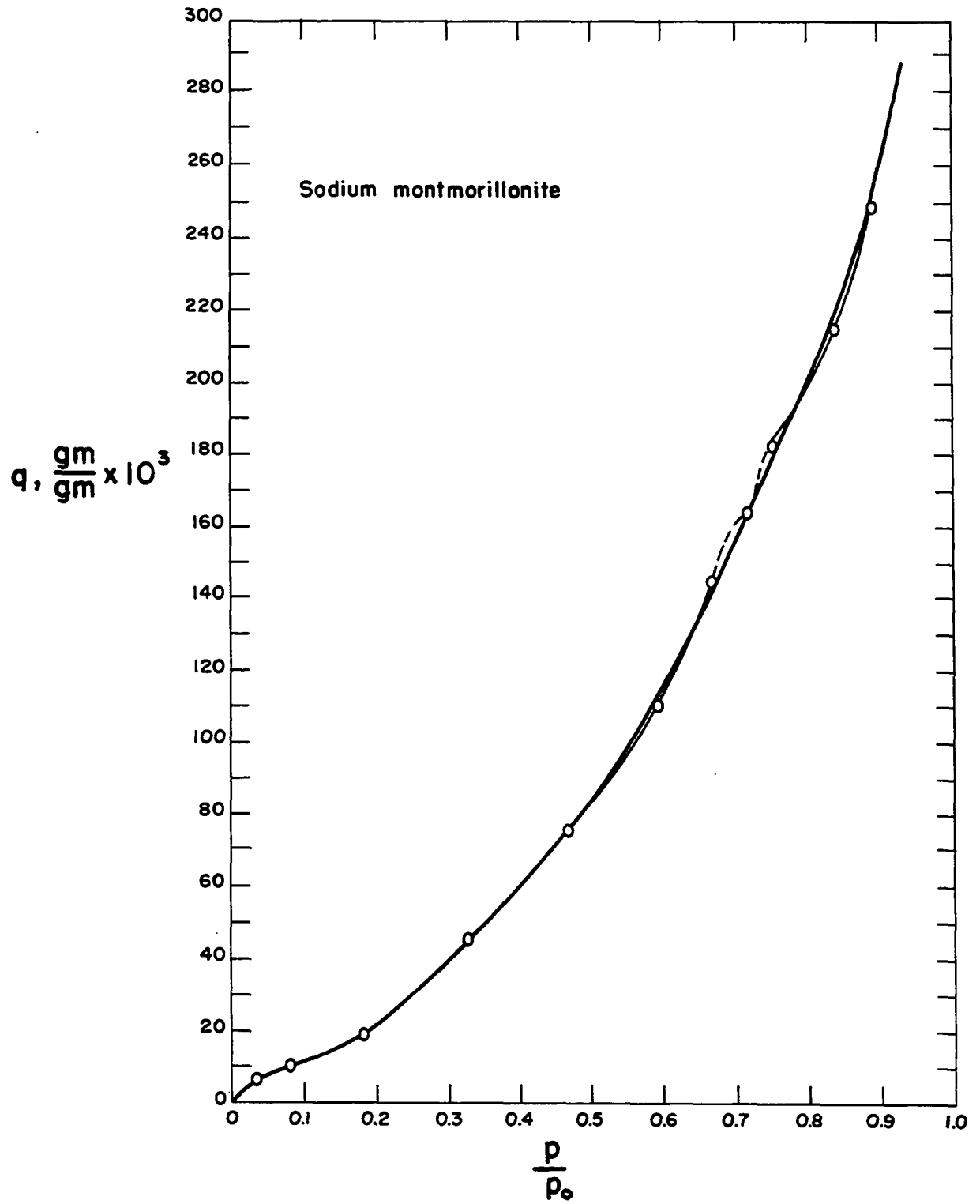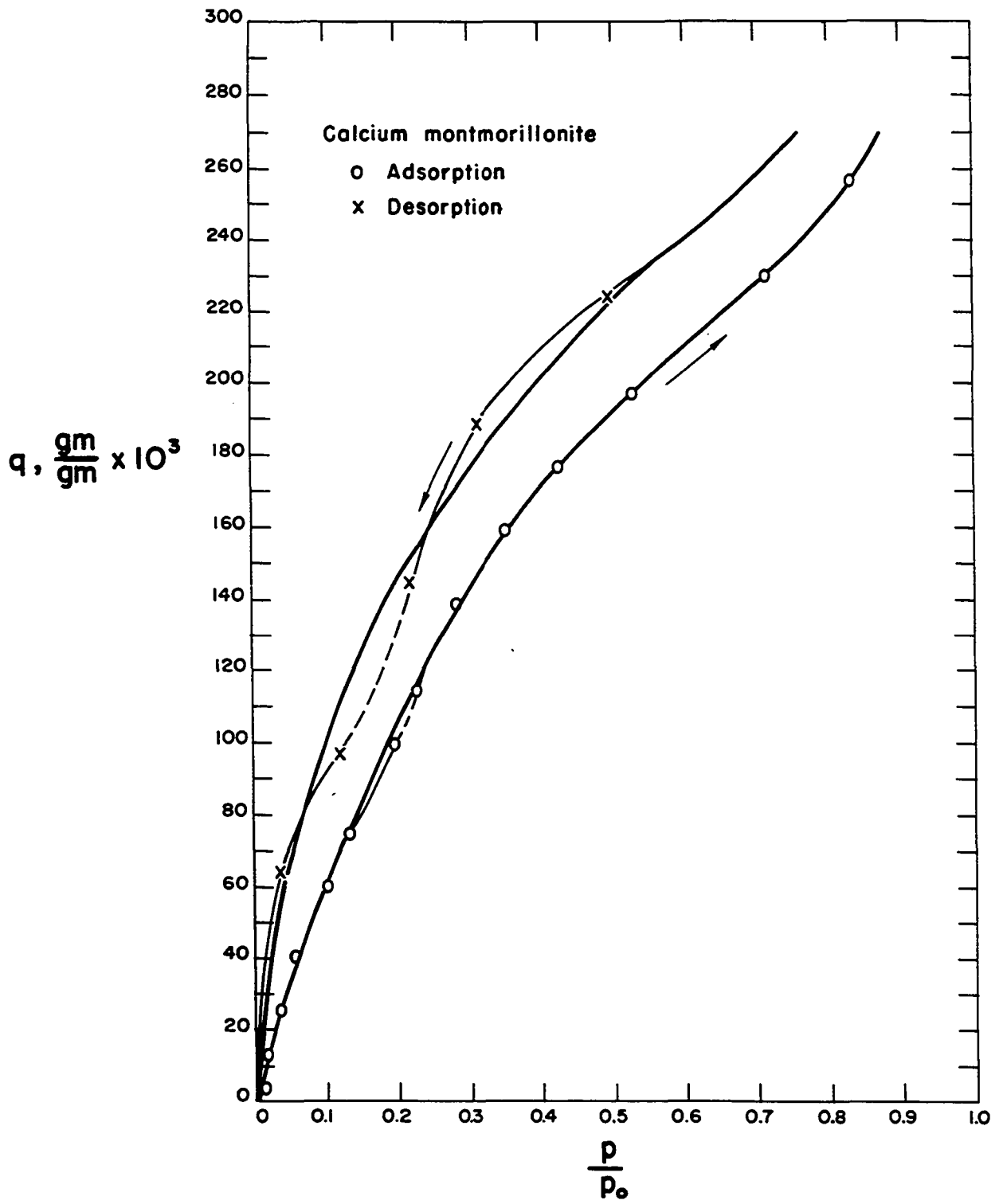   curve

Figure 15.   Adsorption and desorption isotherms of calcium
             montmorillonite represented by smooth curves and
             stepwise curves

molecular layers of water.

X-ray Diffraction

The first order basal spacings, d_{001}, of the sodium montmorillonite and the calcium montmorillonite samples studied were read from X-ray diffraction charts (Figures 11 and 12), and the line broadenings of the peaks corresponding to these spacings were determined as sketched in Figure 16. The 001 spacings and the line broadening thus obtained are plotted against the relative pressures at which they were determined in Figure 17. The 001 spacings for sodium and calcium montmorillonites determined at various relative pressures of water vapor, by Hendricks et al. (32), and Mooney et al. (50) are also included in this figure to obtain a more complete picture. Trends in d_{001} of sodium and calcium montmorillonites are represented in the lower half of the figure by the dashed curves, which show a continuity in the formation of the layers of water molecules. The continuity in the build up of these layers is believed to be due to simultaneous presence of various numbers of water molecule layers (e.g. 0, 1, 2, 3, etc. layers) which results in a gradual average change in platelet separation, and causes interlayer disorders. This is supported by the upper half of Figure 17, which shows large line broadenings corresponding to the steep parts of the d_{001} curves (lower half of Figure 17), and smaller line broadenings

Figure 16. Sketch showing the determination of line breadths
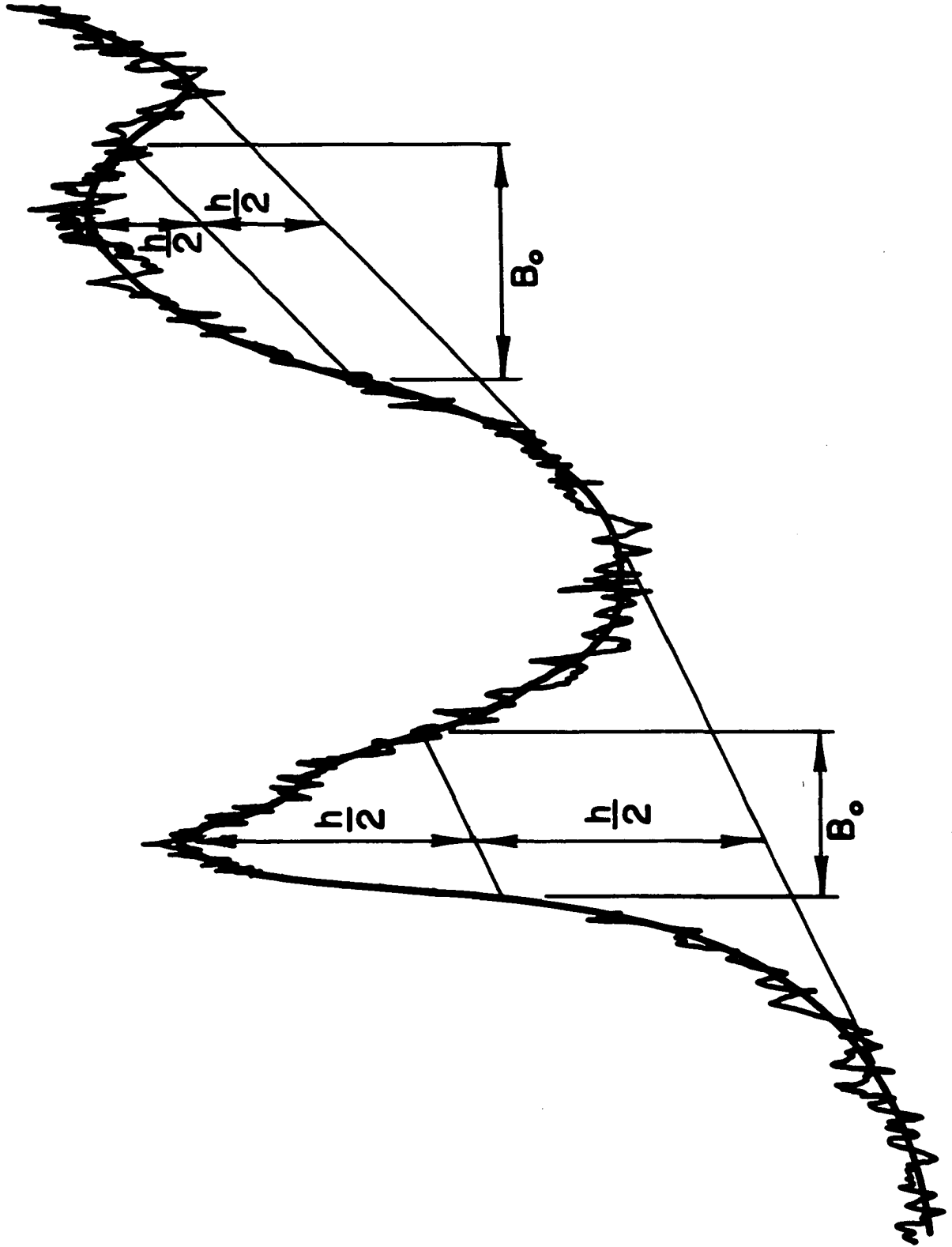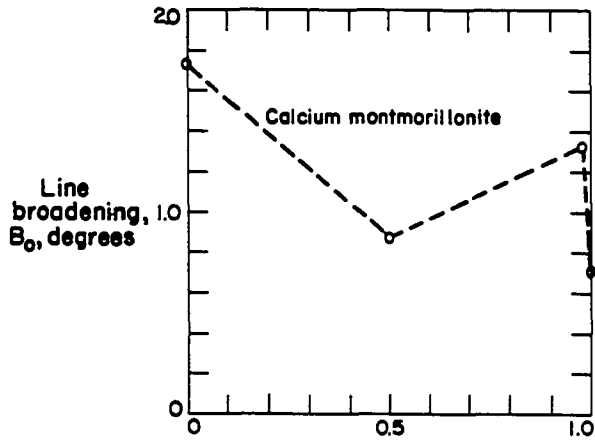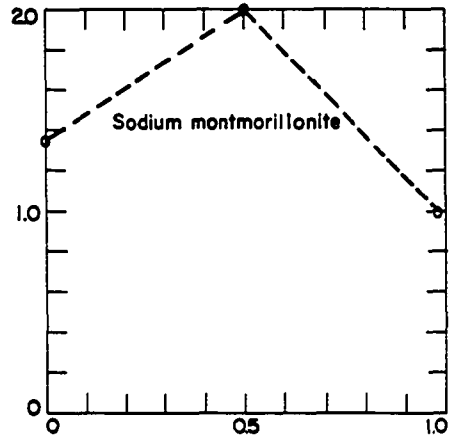of X-ray diffraction peaks

Figure 17. Variations of first order basal spacings and
           line breadths of sodium and calcium mont-
           morillonites with relative pressure of water
           vapor

Line broadening, B_o, degrees — Calcium montmorillonite

Sodium montmorillonite

□ Data of Mooney et. al., for Wyoming montmorillonite
○ Data obtained in the present study

x Data of Hendricks et. al., for Mississippi montmorillonite
▼ Data of Hendricks et. al., for California montmorillonite
▲ Data of Hendricks et. al., for Wyoming montmorillonite

Basal spacing, d, Å

$\frac{p}{P_o}$

$\frac{p}{P_o}$
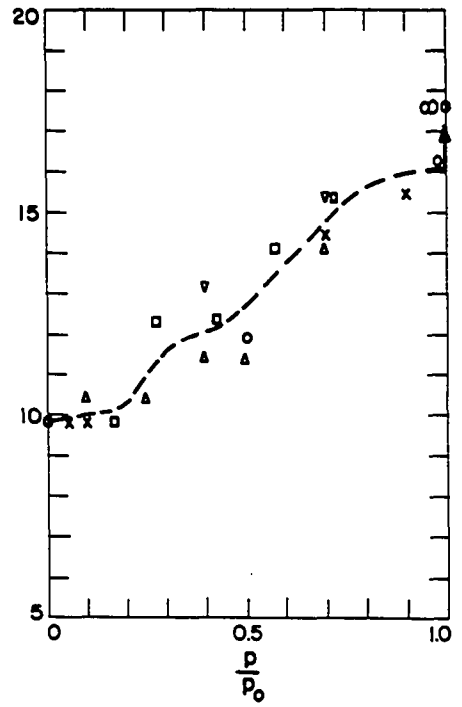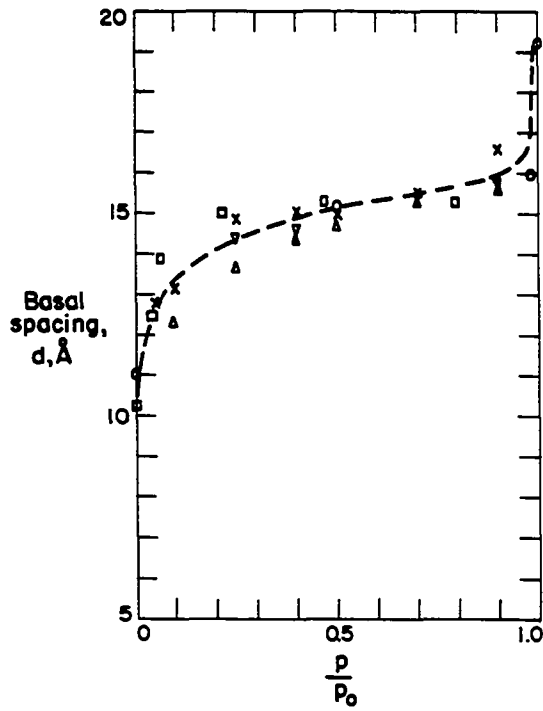
indicative of more uniform interlayer separations (36, p. 517), corresponding to the flat parts of these curves. Further examination of Figure 17 shows that these flat parts occur at spacings corresponding to an integral number of water layers between the platelets 2.76Å being taken as the thickness of a water molecule (53, p. 464). Data of Mooney et al. (50, 42, p. 171) indicate sharper slope variations resulting in almost perfect stepwise curves. Their results were based on data for Wyoming montmorillonite, and on data by Hendricks et al. (32) for Mississippi montmorillonite. The wider sources of data in the present work seem to be responsible for the less definite but probably more representative character of the curves.

It is concluded from spacing changes and line breadths shown in Figure 17 that water molecules enter in between the montmorillonite platelets in a random manner forming 0, 1, 2, etc. molecular layers simultaneously, for relative pressures ranging from zero to an upper limit, the maximum number of the layers and the upper limit of relative pressure being indicated by a rather sudden change of the slope of the d_{001} curves and a sharpening of 001 diffraction peaks. At this upper limit the calculated number of layers almost entirely dominates. With further increase in relative pressure, the next set of layers builds up in a manner similar to the first set and the maximum number of the layers and the upper limit

of the relative pressure for this set of layers are again
indicated by a sudden slope change and a low line broadening
value. Water take-up continues in this manner until the
relative pressure equals 1.

The molecular layers must build up either in laminae, in
which case the stable thicknesses should be an integral mul-
tiple of the diameter of water molecule, or they build in a
spatial geometric arrangement such as ice structure (specu-
lated by several investigators), in which case the layer
thickness should conform to the geometry and the size of water
molecules. Table 6 shows the number of molecular layers of
water in the relative pressure ranges discussed above, esti-
mated on the basis of either laminated stacking or ice struc-
ture. For the reasons to be explained later, it was assumed
that the ice structure starts developing on silica surfaces
of montmorillonite with the hexagonal molecular configuration
of a basal plane of ice (Figure 18A) and proceeds in the fol-
lowing manner: one hexagonal network is shared by two mont-
morillonite platelets causing a separation of 2.76$\overset{\text{o}}{\text{A}}$; two
hexagonal networks are stacked and held by the two silica
surfaces facing each other, causing a separation of 5.52$\overset{\text{o}}{\text{A}}$;
third and fourth molecular layers of water fill in between
the hexagonal network forming tetrahedrons with the water
molecules of the hexagonal network, a complete unit cell of
ice forming with the entrance of the fourth molecular layer

Table 6. Number of molecular layers of water formed between
the platelets of sodium and calcium montmorillonites
when equilibrated at various relative pressures

Mineral	Relative pressure, p/p_0, corresponding to sudden slope change and low line broadening	Number of molecular layers of water between platelets	
		Laminated stacking	Ice configuration
Sodium montmoril- lonite	0	0	0
	0 -0.2	predominantly 0	predominantly 0
	0.2 -0.5	0-1	0-1
	0.5	predominantly 1	predominantly 1
	0.5 -1.0	1-?	1-4
	1.0	?	predominantly 4
Calcium montmoril- lonite	0	predominantly 0	predominantly 0
	0 -0.2	0-2	0-2
	0.2 -0.5	1-2	1-2
	0.5	predominantly 2	predominantly 2
	0.5 -0.9$_7$	2-?	2-4
	0.9$_7$	?	predominantly 4
	0.9$_7$-1.0	?	4-5
	1.0	?	predominantly 5

of water. The latter causes a separation of 7.36Å, which

corresponds to a first order basal spacing of 16.5Å (calcu-

lated from pyrophyllite thickness) or 16.96Å (calculated from

the first order basal spacing of completely collapsed mont-

morillonite). It is further hypothesized that fifth and

sixth molecular layers of water enter between the unit cell

of ice and montmorillonite silica surfaces, forming hexagonal

networks and each causing a further separation of 2.76Å. When

the thickness of the molecular layers of water becomes too

great, very probably the ice structure is destroyed and the water becomes liquid.

Laminated stacking on the other hand causes a separation of 2.76Å for each additional molecular layer of water. Table 6 indicates that the ice configuration explains curves of Figure 17 better than does laminated stacking.

The values of the first order basal spacings calculated from the ice configuration and from laminated stacking of water molecules are compared in Table 7 with the values observed by several investigators and reported by MacEvans (42, p. 195). The calculated values showing agreement with observed values are underlined. This table shows a better agreement with the ice configuration than laminated stacking.

As another alternative for the adsorption mechanism, an arrangement of water molecules with hexagonal closest packing was examined. This arrangement gives a separation of 2.25Å for each additional molecular layer of water, and is least in agreement with observations.

The first order basal spacing, 16.50-16.96Å, calculated for the case of one unit cell of ice adsorbed in between montmorillonite platelets, does not appear in the column of observed spacings (Table 7). On the other hand, Table 6 indicates that this spacing dominates at a relative pressure of 0.9_7 for calcium montmorillonite but is rather sensitive to relative pressure (Figure 17) and also dominates at a relative

Table 7. Comparison of observed first order basal spacings (42, p. 195) of various montmorillonites with those calculated from montmorillonite platelet thickness (c_0), and hypothetical mechanism of the adsorption of water

Observed 1st order spacings, d_{001}, Å	Hypothetical mechanism of water adsorption					
	Ice configuration			Laminated stacking		
	Number of molecular layers of water	Calculated 1st order basal spacing, d_{001}, Å		Number of molecular layers of water	Calculated 1st order basal spacing, d_{001}, Å	
		Based on pyrophyllite thickness	Based on d_{001} of collapsed montmorillonite		Based on pyrophyllite thickness	Based on d_{001} of collapsed montmorillonite
9.5–10.0	0	9.14	9.6_0	0	9.14	9.6_0
12.0–12.4	1	11.90	12.3_6	1	11.90	12.3_6
15.0–15.5	2	14.66	15.1_2	2	14.66	15.1_2
	3	14.66	15.1_2	3	17.42	17.8_8
	4	16.50[a]	16.9_6[a]	4	20.18	20.6
18.4–19.2	5	19.26	19.7_2	5	22.94	23.4_0
21.4–22.5	6	22.02	22.4_8	6	25.70	26.1_6

[a]Corresponds to a single unit cell of ice between platelets.

75

pressure of 1 for sodium montmorillonite but is very sensitive to condensation (Figure 17). Therefore it is hypothesized that the sensitivity to either relative pressure or to condensation makes the single experimental determination of this spacing rather critical. However, Hendricks et al. (32) were able to obtain first order basal spacings of 16.6$\overset{o}{A}$ at 0.90 relative pressure for calcium, barium and hydrogen montmorillonites by single determinations (Table 8). The latter experimental data on one hand and the argument preceding it on the other, indicate that the 16.5$\overset{o}{A}$ first order basal spacing of Table 7, calculated from ice configuration, also agrees with observations.

In Table 7 two values are used for the thickness, c_0, of the montmorillonite platelet, namely the first order basal spacing of completely collapsed montmorillonite and the thickness of the uncharged prototype mineral pyrophyllite. The differences between the two values is 0.46$\overset{o}{A}$, which has been interpreted by Deeds and van Olphen (16) as being the space occupied by exchangeable cations. It is interesting to note that in Table 7 the agreement between the values observed and the values calculated from ice configuration seems to switch from the collapsed montmorillonite basis to the pyrophyllite basis after completion of the unit cell of ice in between the platelets. This may be explained as follows: during the adsorption of the first three molecular layers of water,

exchangeable cations may still occupy the space they had fit in as proposed by Deeds and van Olphen for collapsed montmorillonite but after the formation of the open structure of ice they will have ample space without expanding the structure.

Summing up the discussion of the X-ray study, it may be concluded that the adsorption of the interlayer water is a continuous process, i.e. at equilibrium, 0, 1, 2, ... i layers of adsorbed water molecules coexist in the interlayers and that the adsorbed interlayer water conforms to ice structure. The first of these conclusions indicates that the adsorption is multimolecular, and justifies the use of the BET theory; the second constitutes an apparent experimental support for the hypothesis that interlayer water has ice structure (30, p. 168, 41, 60).

Physical State of Adsorbed Water

The physical state of water held on clay mineral surfaces has attracted the attention of many investigators in various fields (30, p. 162, 59). To postulate a possible physical state for the adsorbed water the attention was focused on the dipole character of water, the hydrogen bond, and the lattice characteristics of the clay mineral surface and the ice crystal.

Hypothetical configuration of adsorbed water

Winterkorn (60) emphasizes the dipole character of water
and states that "The large adsorption forces exerted on water
molecules by the surface of solid soil particles act similar
to externally applied pressures . . .", which agrees with the
basic assumption of the potential theory of adsorption (10,
p. 97). He then postulates on the basis of high pressure
side of the phase diagram of water, that pressures from
adsorption forces, "may liquify solid water or solidify
liquid water". Thus according to Winterkorn the water held
on the surfaces of solid soil particles is in a physical state
corresponding to either liquid water if the moisture content
is high, or to one of the five crystalline forms of ice if
moisture content is low. Apparently, it is assumed that a
single uniform pressure is exerted on the whole of the
adsorbed water, and there is no constraint on the system
other than the ones imposed on the phase equilibrium of one
component water system. This ignores the fact that water is
always present in vapor phase in equilibrium with the adsorbed
phase (liquid or solid) in soil-water systems. Potential
theory on the other hand does not make such assumptions; in
fact, inherent in the theory is the additional constraint
imposed by the adsorptive surface, which gives rise to the
formation of layers in the adsorption space separated from
each other by equipotential surfaces the last layer being in

equilibrium with the vapor phase (10, p. 97).

Hendricks and Jefferson (31), basing their argument on hydrogen bonding, dipole character of water, and lattice characteristics of the clay mineral surface, suggest that adsorbed water molecules are joined by hydrogen bonding into hexagonal groups of an extended hexagonal net. This net can be formed by bringing the offset water molecules of the ice structure into the same plane by stretching the ice structure shown in Figure 24B. By assuming $3.0\overset{\circ}{A}$ for the separation of oxygen atoms, they showed that the net has the $\underline{a}$ and $\underline{b}$ dimensions of the clay minerals, and every other water molecule in the net has one hydrogen available for hydrogen bonding and lies over an oxygen of the clay mineral surface. On this basis they hypothesize that the hexagonal net of water molecules is hydrogen bonded to the clay mineral surface, and successive hexagonal nets build up on each other by being hydrogen bonded to the previous one. This gives a laminated stacking causing a separation of $2.76\overset{\circ}{A}$ for each molecular layer of water, with four water molecules per molecular layer per unit cell. Each water molecule in a monomolecular layer of this arrangement covers an area of about $11.5\overset{\circ}{A}^2$.

Macey (41), observing the lattice similarities between the basal planes of ice and of clay minerals, postulated that the ice structure starts developing on clay mineral surfaces with the hexagonal molecular configuration of the basal plane

of ice (Figure 18A and 19A). Distance between adjacent water molecules in the hexagonal basal plane of ice is 4.52$\overset{o}{A}$ and the distance between appropriate oxygen atoms in the silica surface is 4.51$\overset{o}{A}$. Indeed as stated by Macey, "The ice structure fits almost perfectly upon that of the silicate". There are 2 2/3 molecules of water per unit cell in a mono-molecular layer having this structure[*] and each water molecule covers an area of about 17.5$\overset{o}{A}{}^2$. Although the fit between the matching oxygen atoms of the silica surface and the water molecules of ice crystal is perfect, one fourth of the water molecules lie over the hexagonal holes of the net of oxygen atoms of the silica surface. Question may rise as to how these molecules are held in these positions; however, the hexagonal net of water molecules is confronted either by the silica surface of the next clay mineral platelet or by an-other hexagonal net of water molecules which in turn is matched by a clay mineral platelet. Thus the water molecules lying over hexagonal holes may be matched and held in these positions by the water molecules of the next hexagonal net and/or the oxygen atoms of the next clay mineral platelet. This would result in regular offset in the stacking of the clay mineral platelets, decreasing hk intensities and giving the possibility for a repeating double or triple-layer

---

[*]According to Grim (30, p. 169) the number of water molecules per unit cell for this structure is 3.

Figure 18. Ice structure; dark spheres represent the
arrangement of water molecules held by clay
surface, as they stand in ice structure (A)
according to Macey, (B) according to
Hendricks and Jefferson

Figure 19. Arrangement of water molecules on montmoril-
lonite surface (A) according to Macey, (B)
according to Hendricks and Jefferson
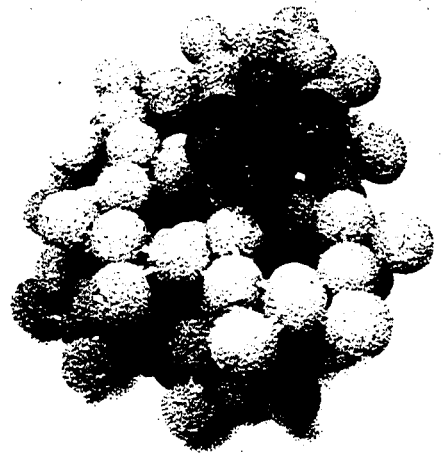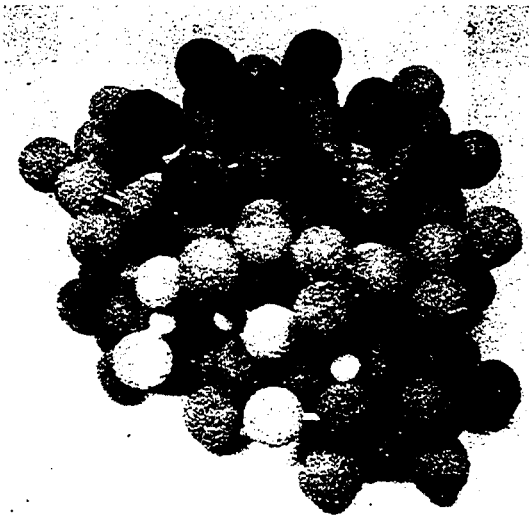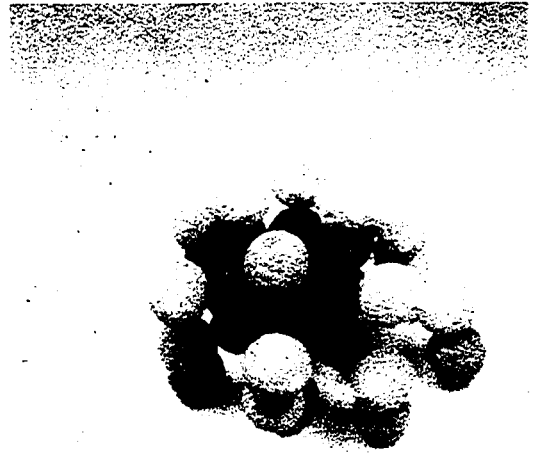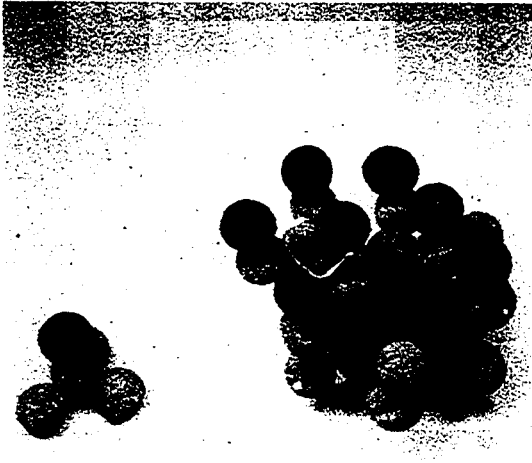
structure including organized water molecules. In mont-
morillonite the absence or extreme broadness of many hk
reflections as compared to muscovite may be cited as a justi-
fication of this offset stacking. Another evidence may be
seen in the diffraction charts (Figures 11 and 12), which
show peaks at an angle corresponding to a spacing about twice
the d_{001}, indicating a superlattice, or organized secondary
lattice differences between the unit cells. Superstructures
have been reported with other clay minerals (9, pp. 93-96,
251, 367 and 374); but not for montmorillonite, probably be-
cause of the large superlattice spacing, which would not be
resolved in studies as customarily conducted with copper
radiation. The use of the longer wave length chromium radi-
ation allowed such spacings to be observed. The presence of
a superlattice suggests that the offset stacking of platelets
to match water molecules with the oxygen atoms of the silica
surface must repeat in the c-axis direction in an organized
manner.

The ice structure may develop in the interlayer spaces
in two ways. The first of these, which consists of building
the ice structure by filling water molecules in between the
two surfaces of the unit cell of ice formed on the surfaces
of two platelets, was discussed earlier and found to agree
with the actual d_{001} spacing observations. The second way
is to stack the hexagonal rings in the way they appear suc-

cessively in the quartz-like structure of ice. This second way would cause an alternating platelet separation of $2.76\overset{o}{A}$ and $0.92\overset{o}{A}$ in successive steps with the entrance of each molecular layer of water, which does not agree with the observed increments of first order basal spacings. This method of stacking results in an arrangement very similar to the one suggested by Hendricks and Jefferson, except that in the latter arrangement the two layers (planes of hatched and circled spheres in Figure 19B) are stretched so all water molecules are brought onto one plane instead of being distributed between two layers; putting all water molecules on one surface by stretching reduces the effective area occupied by one water molecule from $17.5\overset{o}{A}^2$ to $11.5\overset{o}{A}^2$.

Forslind (23, 24) suggests the very same ice structure arrangement suggested by Macey but he bases his argument on the Edelman-Favejee structure (42, p. 152) instead of Hofman-Endell-Wilm structure (42, p. 146) for montmorillonite, observing that all of the water molecules of the basal plane of ice could be matched with the oxygen atoms of silica surface of the Edelman-Favejee structure. He also cites electron diffraction photographs supporting ice structure arrangement, but these data were questioned because the adsorbed water should have been removed by the high vacuum (42, p. 172). The Edelman-Favejee structure also has been precluded rather recently by studies based on Fourier

syntheses (42, p. 300).

Barshad (5), correlating dehydration data with lattice expansion, suggests another arrangement of water molecules, which becomes progressively denser with the addition of monomolecular layers of water. For the first monomolecular layer he suggests two alternative arrangements. The first of these builds up when water molecules form tetrahedra with the bases of the linked silica tetrahedra of the lattice; this configuration among others suggested by Barshad, corresponds to loose packing with four molecules of water per unit cell, each water molecule covering an area of about $11.5\overset{o}{A}^2$. The second alternative suggested by Barshad is the formation of a closer packing of water molecules arranged in hexagonal rings in the same manner as the oxygens of the bases of the linked silica tetrahedra; in this arrangement there are six water molecules per unit cell and each molecule covers an area of about $7.7\overset{o}{A}^2$.

Density of adsorbed water

Attention has been focused on the accurate determination of the density of adsorbed water to provide experimental evidence for or against the configurations proposed. Two limitations arise in the use of density for providing this evidence; the first is the experimental difficulties involved in density determinations and the second is the uncertainty

involved in the estimation of the number of monomolecular layers present and their distribution in interlayer spaces or on external surfaces at the time of density determination. For instance, the density of adsorbed water formed by ice structure as proposed in this study would be

$$\rho_1 = \frac{3 \times 18.0 \times 10^{24}}{6.02 \times 10^{23} \times 4.52 \times 3.91 \times 3 \times 2.76} = 0.62 \text{ gm/cc}$$

for the first complete monomolecular adsorbed layer. The calculation is based on the following relationship

$$\rho = \frac{n\,M}{NSh}$$

where ρ is the density of adsorbed water, n is the number of water molecules adsorbed per unit cell base area of ice, M is the molecular weight of water, N is the Avogadro constant, S is the base area of the unit cell of ice, and h is the total thickness of the adsorbed molecular layers of water. Before the completion of the first monomolecular layer the average density of the adsorbed water would be less than 0.62 gm/cc. The density of two, three and four adsorbed molecular layers of the proposed arrangement would be

$$\rho_2 = \frac{6 \times 18.0 \times 10^{24}}{6.02 \times 10^{23} \times 4.52 \times 3.91 \times 3 \times 2 \times 2.76} = 0.62 \text{ gm/cc}$$

$$\rho_3 = \frac{9 \times 18.0 \times 10^{24}}{6.02 \times 10^{23} \times 4.52 \times 3.91 \times 3 \times 5.52} = 0.92 \text{ gm/cc}$$

and

$$\rho_4 = \frac{12 \times 18.0 \times 10^{24}}{6.02 \times 10^{23} \times 4.52 \times 3.91 \times 3 \times 7.36} = 0.92 \text{ gm/cc}$$

respectively. As mentioned earlier, hexagonal Macey rings can be stacked in another pattern, namely in the way they appear successively in ice structure. With this latter mode of stacking densities would be 0.62, 0.93, 0.79 and 0.92 gm/cc for one, two, three and four molecular layers of water, respectively. The density of the adsorbed water for Hendricks-Jefferson arrangement would be 0.94 gm/cc. It would be again 0.92 gm/cc for the loosest Barshad arrangement. Recent experimental values published for the density of water adsorbed on montmorillonite range from 0.75 to 0.996 gm/cc (1, 7, 16). Bradley (7), using the data reported in literature, has shown that the density of adsorbed water decreases as the water content of the mineral decreases, following a smooth curve. These experimental density values only indicate that the adsorbed water should have a loose structure as postulated by the investigators mentioned above, but does not tell with any certainty which of the suggested arrangements could be considered real; the low density values may be due to incomplete monomolecular layers whereas the high density values may be due to complete monomolecular layers as well as to multimolecular layers arranged according to any of the suggested configurations.

It appears that the investigation conducted by De Wit and

Arens (18) on the density of water-clay pastes has caused some confusion in the literature. These investigators calculated the specific volume of the adsorbed water from the water-clay paste densities. The results of their calculations seem rather unrealistic since they have used an extremely low density (2.348 gm/cc) for dehydrated montmorillonite, but they obtained an average specific volume of about 0.73 cc/gm for water adsorbed on montmorillonite at moisture contents between 11.6% and 28.4%. References to this work evidently interpreted the results in different ways. Grim (30, p. 171) cites their results as an experimentally determined density of 0.73 gm/cc for water adsorbed by clay minerals without any further comments. Bradley (7), using De Wit and Arens' paste density data, recalculated specific volumes based on a density of 2.83 gm/cc for dehydrated montmorillonite, and for the adsorbed water at a moisture content of 11.6% got 1.33 cc/gm which corresponds to a density of 0.75 gm/cc. Mackenzie (43) cites the specific volume data of De Wit and Arens (0.73 cc/gm or 1.4 gm/cc) as an evidence for dense packing of water molecules adsorbed on clay minerals.

On account of the extremely low density for dehydrated montmorillonite used by De Wit and Arens, Bradley's recalculated specific volume values seem to be more representative, supporting a loose packing of water molecules adsorbed by

montmorillonite.

BET Parameters

To furnish experimental evidence for the arrangement of water molecules adsorbed on montmorillonite, a different approach was used in the present work. This approach consists of the determination of the area occupied by one water molecule from adsorption isotherm data by using the BET equation (equation 9a) as it has been utilized by others to determine the cross-sectional areas of organic molecules adsorbed on graphite (15).

The BET plots of the sorption data of water vapor on sodium and calcium montmorillonites (Tables 2, 3, 4 and 5) are given in Figures 20 and 21, respectively.

Sodium montmorillonite

The BET plot of the adsorption data for sodium montmorillonite (Figure 20) shows discontinuities, one at a relative pressure of about 0.2 and probably a second at a relative pressure between 0.6 and 0.7. As discussed earlier, the relative pressures 0.2 and 0.7 approximately correspond to the beginning and the completion of the first monolayer of interlayer water, respectively. On this basis it was concluded that the BET plot in the relative pressure range below 0.2 represents the adsorption taking place predominantly

Figure 20. BET plots of the sorption data of water vapor on sodium montmorillonite

Figure 21.   BET plots of the sorption data of water vapor
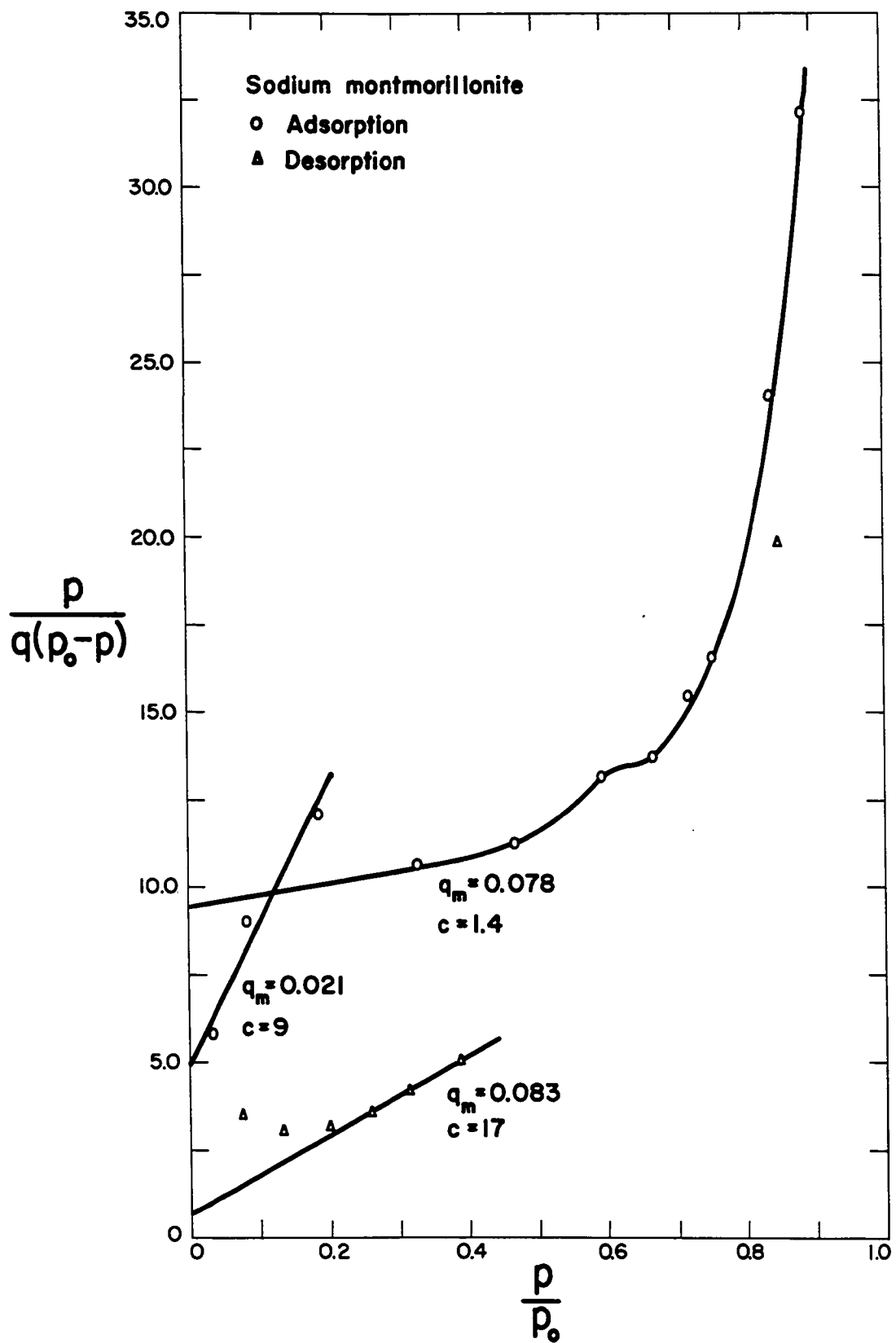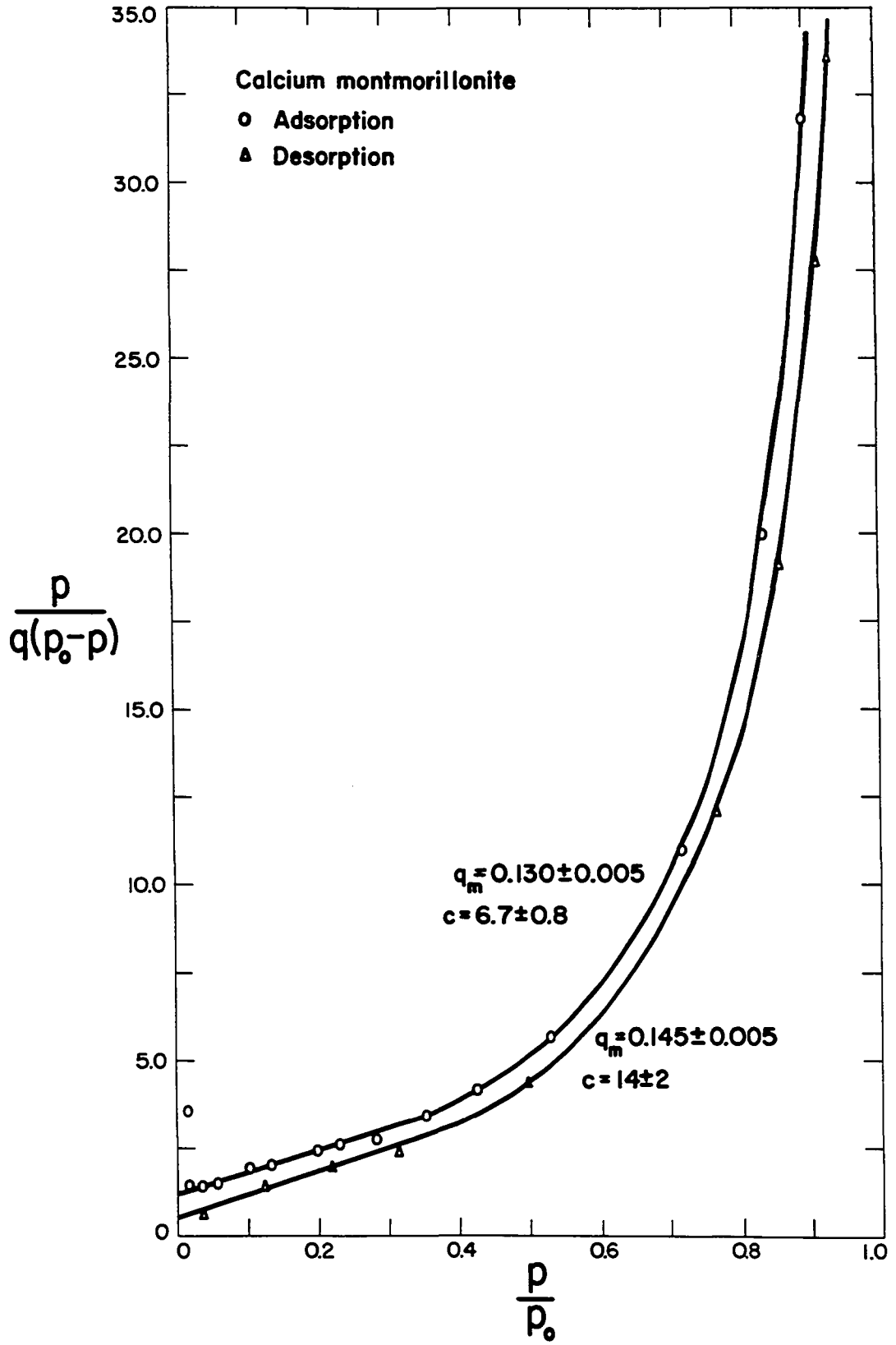   on calcium montmorillonite

Calcium montmorillonite
o Adsorption
△ Desorption

$q_m = 0.130 \pm 0.005$
$c = 6.7 \pm 0.8$

$q_m = 0.145 \pm 0.005$
$c = 14 \pm 2$

$\dfrac{p}{q(p_o - p)}$

$\dfrac{p}{p_o}$

on the external surfaces, and the BET parameters q_m and C obtainable from the linear BET plot within this pressure range represent the external surfaces. The numerical values obtained for q_m and C are given in the figure. The external surface area could be calculated from q_m if the cross sectional area of the water molecule were known. As discussed above, experimental evidences point toward a loose packing of water molecules on clay mineral surfaces, making questionable the generally accepted cross-sectional area value of 10.8$\overset{o2}{A}$ (49) based on closest packing. The relative pressure range of 0.2 to 0.7, representing adsorption on all surfaces, leaves little margin for the so-called BET relative pressure range (0.05 to 0.3) in which the BET plot is expected to be linear. To estimate q_m and C for all surfaces, the second part of the BET plot was extrapolated to low pressures, producing a straight line in the BET range. The numerical values of q_m and C obtained from this straight line are given in the figure. The BET plot of desorption data is also included in Figure 20 for comparison, since it has been suggested and used by others (49) for evaluation of the BET parameters. The parameter q_m estimated from Figure 20 for all surfaces is 0.078 gram per gram of sodium montmorillonite including the monomolecular interlayer water, and it is 0.021 gram per gram of sodium montmorillonite not including interlayer water, i.e., adsorbed only on external surfaces. Therefore the mono-

molecular interlayer water held simultaneously by two plate-
lets is 0.078 - 0.021 = 0.057 gram per gram of sodium mont-
morillonite. From these quantities, a fictitious q_m for a
complete monomolecular layer of water covering all surfaces
independently can be calculated as follows (49, 61):

$$q_{mf} = 2 (q_{mt} - q_{me})$$

$$= 2 \times 0.057 + 0.021 = 0.135 \text{ gm/gm},$$

where q_{mf} is the fictitious BET parameter, and q_{mt} and q_{me}
are experimentally determined BET parameters for all surfaces
and for external surfaces respectively. From the value of q_{mf}
and crystallographic specific surface of sodium montmorillonite
the cross-sectional area of water molecule adsorbed on sodium
montmorillonite can be calculated by using equation 11. The
crystallographic specific surface for sodium montmorillonite
was calculated from the formula weight and dimensions of its
unit cell by using the following equation:

$$\Sigma = \frac{N}{M} \sigma$$

where Σ is the specific surface, N is the Avogadro constant,
M is the formula ($Al_{3.34} Mg_{0.06} Si_8 O_{20} (OH)_4 Na_{0.66}$) weight
of the unit cell and σ is the area exposed by one unit cell.
M is equal to 742 and σ is equal to $2 \times 5.16 \times 8.94 Å^2$ where
$5.16 Å$ and $8.94 Å$ are the unit cell dimensions a_0 and b_0,
respectively, calculated from d_{060}. Substituting these
values into the above equation, the following was obtained
for the specific surface:

$$\frac{6.02 \times 10^{23}}{742} \frac{2 \times 5.16 \times 8.94}{10^{20}} = 748 \ m^2/gm$$

Substituting this value and the value of q_{mf} into equation 11, the following is obtained

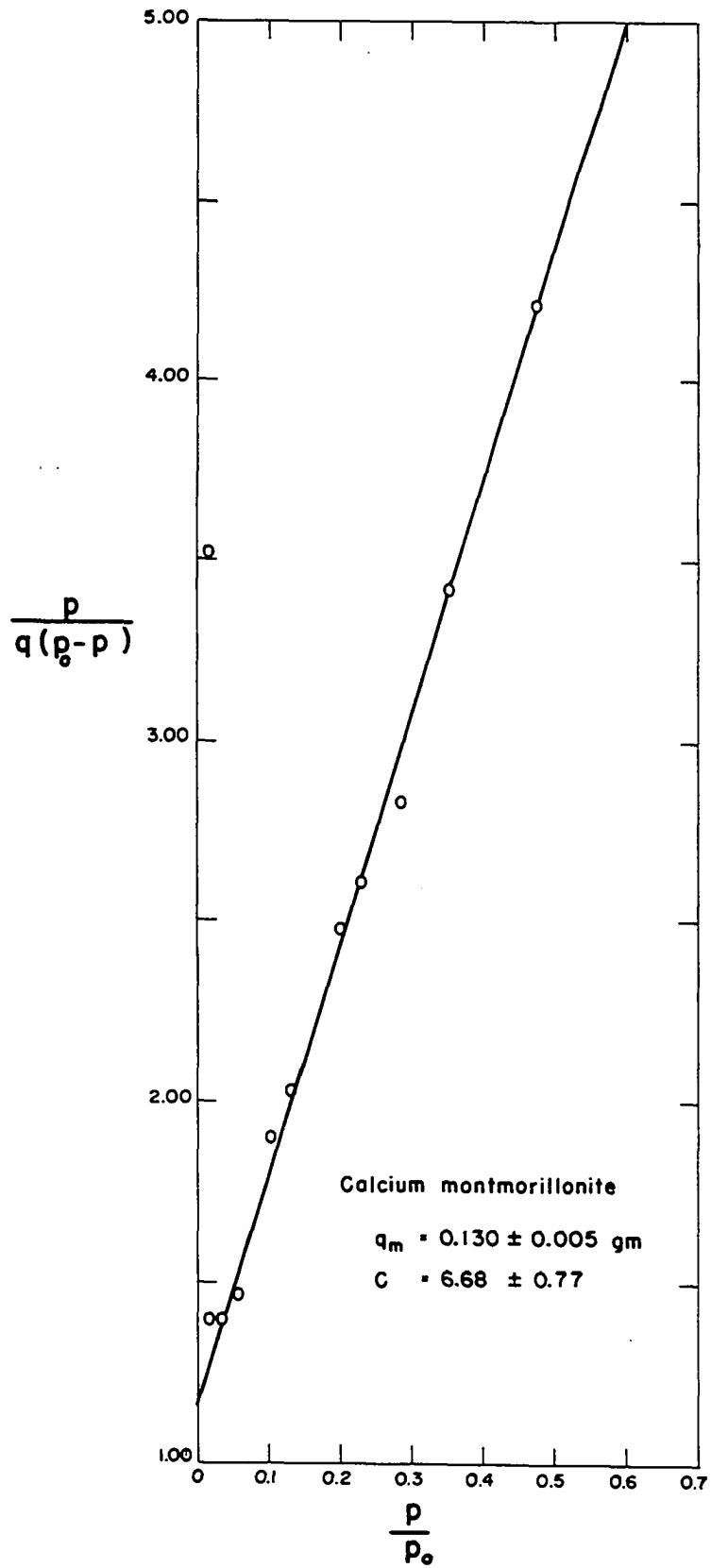$$748 = \frac{6.02 \times 10^{23} \times 0.135}{18.0} \ s$$

from which the cross-sectional area of water molecule adsorbed on sodium montmorillonite is obtained in $\overset{o2}{A}$ as follows:

$$s = \frac{748 \times 18.0}{6.02 \times 10^{23} \times 0.135} \times 10^{20} = 16.6\overset{o2}{A}$$

Calcium montmorillonite

The BET plot of the adsorption data of water for calcium montmorillonite constitutes a straight line within the BET range (Figure 21), as would be expected from the results of X-ray investigation, which indicated the entrance of two molecular layers of interlayer water within the BET relative pressure range. Therefore the parameter q_m obtainable from the linear BET plot represents a complete monomolecular layer of water covering all surfaces independently. The BET plot of desorption data is also included in Figure 21 for comparison. The straight line portion of the adsorption curve of Figure 21 is reproduced in Figure 22. By varying the position of the straight line within the limits of experimental errors discussed earlier, a value of 0.130 ± 0.005 grams per gram of calcium montmorillonite was obtained for

Figure 22. Straight line BET plot of the adsorption data
of water vapor on calcium montmorillonite

Calcium montmorillonite

q_m = 0.130 ± 0.005 gm

C = 6.68 ± 0.77

q_m. (An error calculation was not possible for sodium mont-
morillonite because of the approximation made in plotting.)
From this value of q_m and calculated crystallographic specific
surface, the cross-sectional area of one water molecule
adsorbed on calcium montmorillonite was calculated from
equation 11 as follows:

$$s = \frac{752 \times 18.0}{6.02 \times 10^{23} \times 0.130} \times 10^{20} = 17.3 \pm 0.7 Å^2$$

Since several approximations had to be made to obtain the
cross-sectional area of a water molecule adsorbed on sodium
montmorillonite the calculation with calcium montmorillonite
is more dependable. Nevertheless, the agreement between the
two values is very good.

BET plots from previous work

The adsorption isotherm and X-ray diffraction data of
Hendricks et al. (32) are tabulated in Table 8. The values
of the BET function, $\frac{p}{q(p_o - p)}$, were calculated from the
adsorption isotherm data of each montmorillonite studied by
them, and are included in this table. The BET plots con-
structed using these data, and the BET parameters q_m and C
calculated from the linear branches of these plots are given
in Figures 23, 24 and 25. The values of the parameter q_m
obtained can be divided into two groups, q_m values for the
first group varying between 0.023 and 0.100 grams per gram of

Table 8. Adsorption isotherm data of Hendricks et al. (32)

Mineral	p/p_0	q, $\frac{gm}{gm} \times 10^3$	$\frac{p}{q(p_0-p)}$	d_{001}, Å
Magnesium	0.05	85	0.62	13.5
saturated	0.10	115	0.97	13.5
Mississippi	0.25	160	2.08	14.1
montmorillonite	0.40	195	3.42	14.4
	0.50	220	4.55	15.5
	0.70	270	5.63	15.8
	0.90	340	26.5	15.3
Calcium	0.05	70	0.75	12.8
saturated	0.10	105	1.06	13.2
Mississippi	0.25	160	2.08	14.9
montmorillonite	0.40	200	3.33	15.0
	0.50	220	4.55	15.0
	0.70	270	8.63	15.5
	0.90	360	25.0	16.6
Strontium	0.05	50	1.05	12.1
saturated	0.10	85	1.31	12.3
Mississippi	0.25	140	2.38	13.2
montmorillonite	0.40	200	3.33	15.1
	0.50	220	4.55	15.5
	0.70	260	8.96	15.5
	0.90	340	26.5	15.5
Barium	0.05	50	1.05	11.9
saturated	0.10	75	1.48	12.0
Mississippi	0.25	110	3.03	12.21
montmorillonite	0.40	140	4.76	12.4
	0.50	160	6.25	13.2
	0.70	230	10.1	15.7
	0.90	320	28.1	16.6
Lithium	0.05	65	0.81	12.3
saturated	0.10	85	1.31	12.3
Mississippi	0.25	120	2.78	12.3
montmorillonite	0.40	155	4.30	13.0
	0.50	170	5.88	13.0
	0.70	240	9.71	15.0
	0.90	340	26.5	15.5

Table 8. (Continued)

Mineral	p/p_0	$\frac{gm}{gm}$ q, x 10^3	$\frac{p}{q(p_0-p)}$	d_{001}, Å
Hydrogen	0.05	45	1.17	diffuse
saturated	0.10	75	1.44	12.3
Mississippi	0.25	130	2.56	diffuse
montmorillonite	0.40	165	4.04	13.8
	0.50	190	5.26	14.4
	0.70	250	9.32	15.8
	0.90	360	25.0	16.6
Sodium	0.05	25	2.10	9.8 diffuse
saturated	0.10	40	2.79	9.8 diffuse
Mississippi	0.25	65	5.13	diffuse
montmorillonite	0.40	105	6.35	diffuse
	0.50	120	8.33	diffuse
	0.70	175	13.3	14.4 diffuse
	0.90	280	32.1	15.5
Potassium	0.05	15	3.51	
saturated	0.10	30	3.70	
Mississippi	0.25	55	6.06	11.4
montmorillonite	0.40	80	8.33	11.9
	0.50	100	10.0	11.9
	0.70	140	16.6	11.9 diffuse
	0.90	200	45.0	11.9 diffuse
Cesium	0.05	20	2.63	
saturated	0.10	40	2.78	diffuse
Mississippi	0.25	65	5.13	diffuse
montmorillonite	0.40	80	8.33	diffuse
	0.50	95	10.5	diffuse
	0.70	125	18.6	diffuse
	0.90	180	50.0	diffuse
Calcium	0.05	35	1.50	12.8 diffuse
saturated	0.10	120	0.93	13.2 diffuse
California	0.25	150	2.22	14.4
montmorillonite	0.40	190	3.51	14.6
	0.50	260	3.85	14.8
	0.70	320	7.28	15.4
	0.90	460	19.5	15.7

Table 8. (Continued)

Mineral	p/p_0	q, $\frac{gm}{gm} \times 10^3$	$\frac{p}{q(p_0-p)}$	d_{001}, Å
Sodium	0.05	25	2.10	
saturated	0.10	50	2.22	9.8 diffuse
California	0.25	90	3.70	diffuse
montmorillonite	0.40	130	5.13	13.2 diffuse
	0.50	180	5.56	
	0.70	270	8.63	15.4
	0.90	440	20.5	15.5
Calcium	0.05	40	1.32	
saturated	0.10	60	1.85	12.3
Wyoming	0.25	105	3.17	13.6
montmorillonite	0.40	145	4.60	14.4
(Volclay)	0.50	155	6.45	14.8
	0.70	190	12.3	15.4
	0.90	240	37.5	15.6
Sodium	0.05	5	1.05	
saturated	0.10	15	7.40	10.4 diffuse
Wyoming	0.25	25	13.3	10.4 diffuse
montmorillonite	0.40	60	11.1	11.4 diffuse
(Volclay)	0.50	80	12.5	11.4 diffuse
	0.70	140	16.6	14.2 diffuse
	0.90	220	40.9	diffuse

the mineral, and those for the second varying between 0.125 and 0.138 grams per gram of the mineral. Examination of the first order basal spacings given in Table 8 indicates that for the first group the BET range matches the relative pressure range at which either no interlayer water or only one molecular layer of interlayer water exists, as was the case for sodium montmorillonite investigated in the present study. This defies a direct analysis to obtain the BET parameter q_m.

Figure 23.   BET plots of the adsorption data of Hendricks
              et al. (32) for monovalent cation saturated
              Mississippi montmorillonite
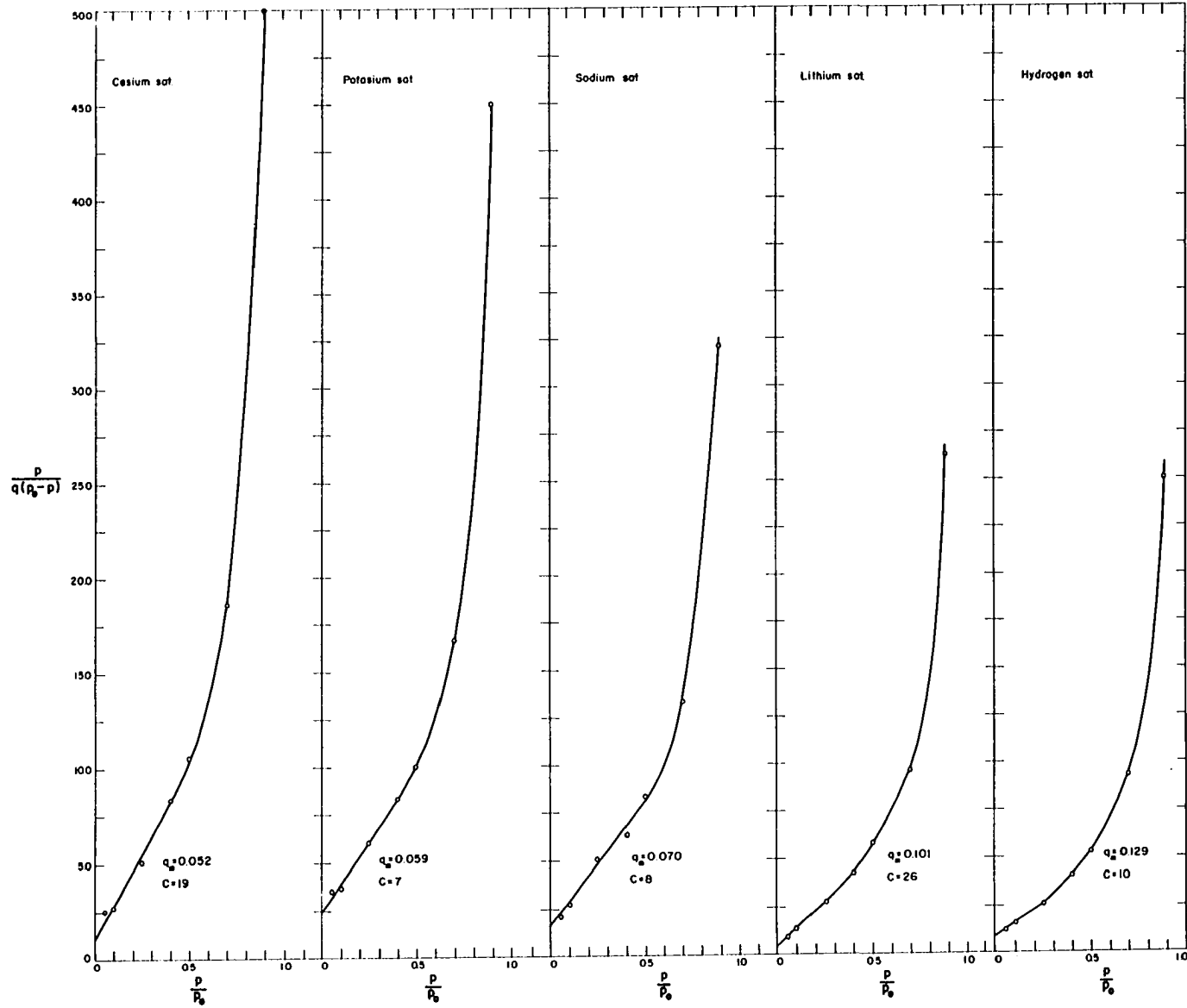
Mississippi montmorillonite

Figure 24. BET plots of the adsorption data of Hendricks
et al. (32) for divalent cation saturated
Mississippi montmorillonite
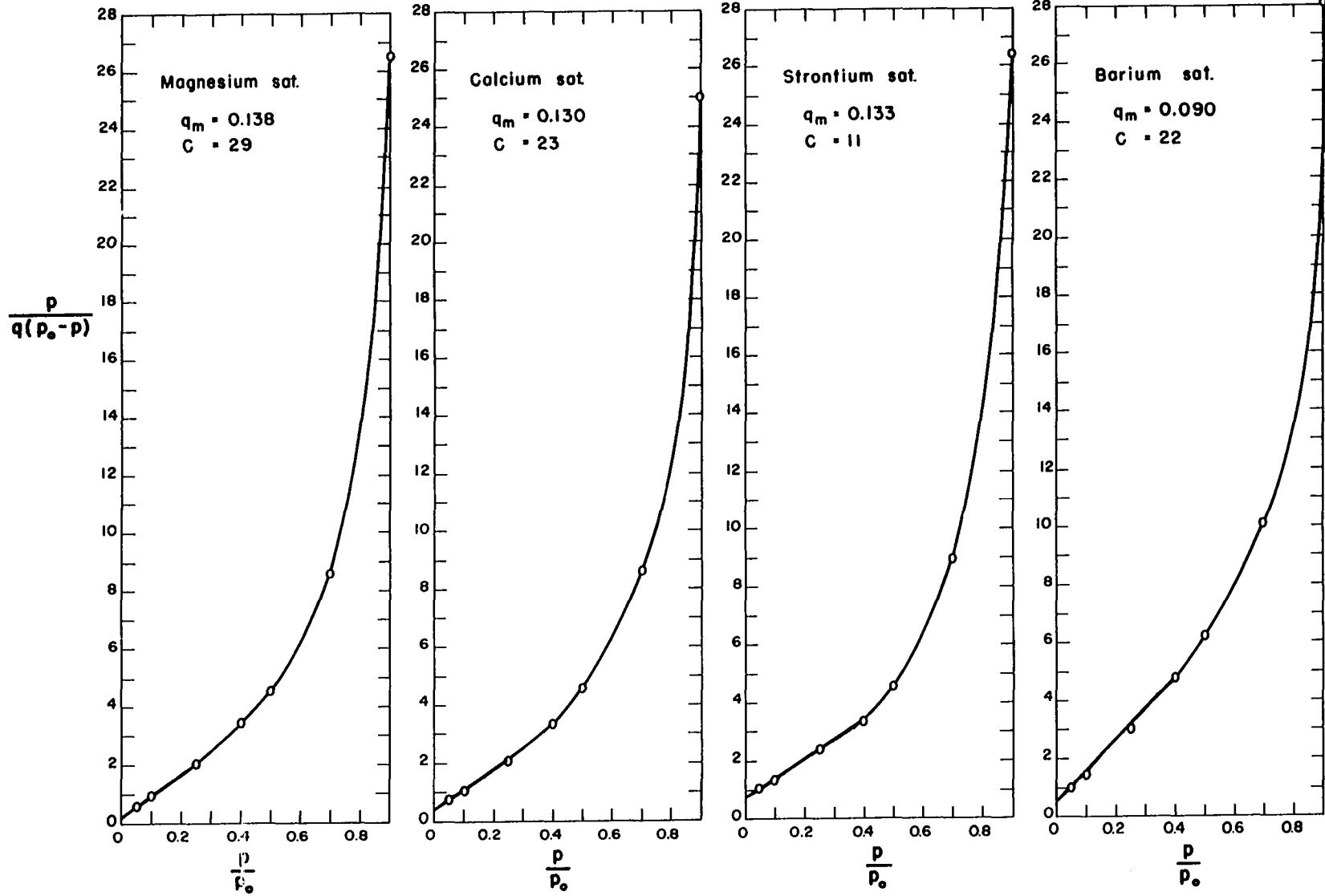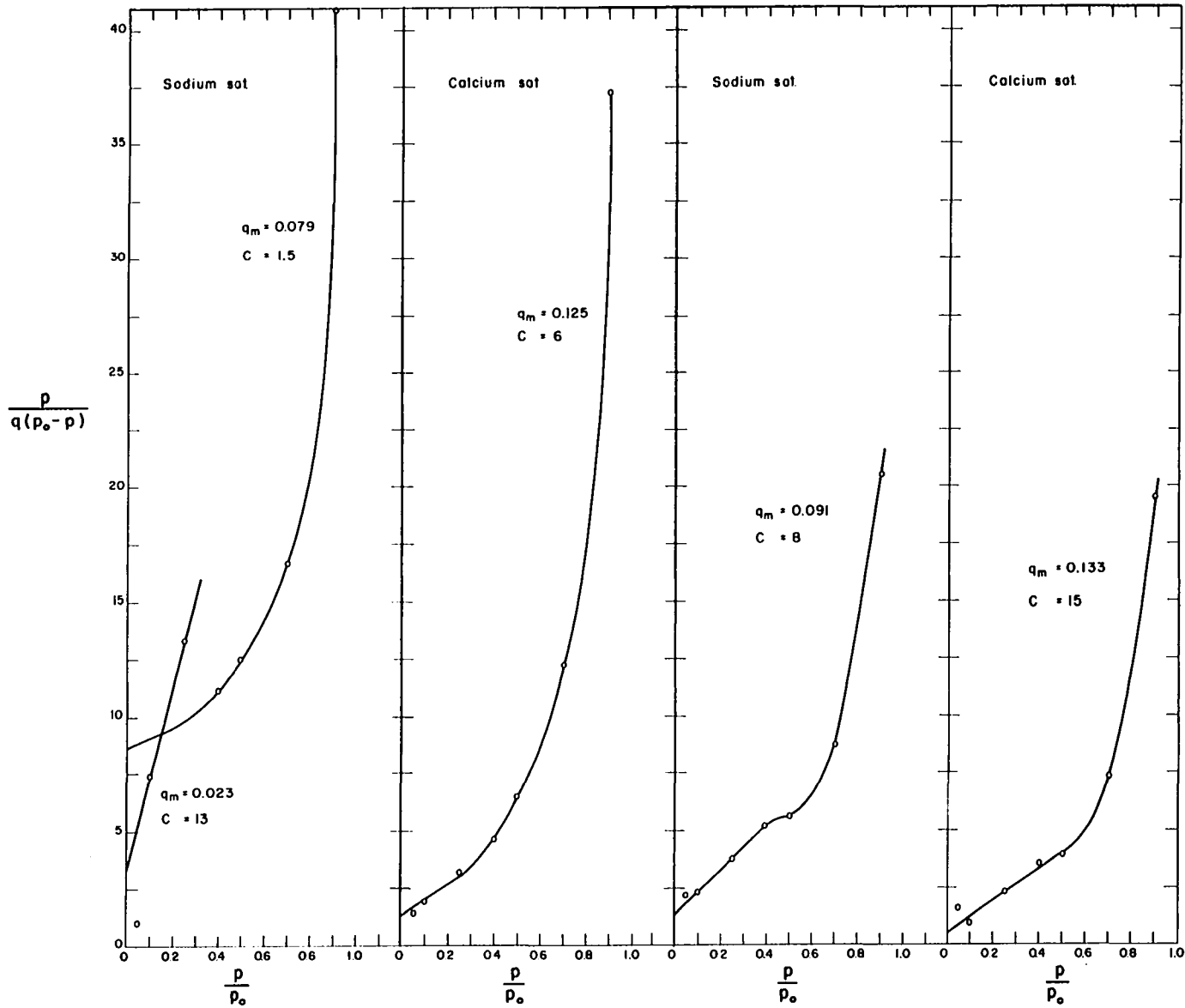
Mississippi Montmorillonite

Magnesium sat.

$q_m = 0.138$
$C = 29$

Calcium sat

$q_m = 0.130$
$C = 23$

Strontium sat.

$q_m = 0.133$
$C = 11$

Barium sat.

$q_m = 0.090$
$C = 22$

$\dfrac{p}{q(p_o - p)}$

$\dfrac{p}{p_o}$

$\dfrac{p}{p_o}$

$\dfrac{p}{p_o}$

$\dfrac{p}{p_o}$

Figure 25. BET plots of the adsorption data of Hendricks
            et al. (32) for monovalent and divalent cation
            saturated Wyoming and California montmorillonites

For the second group, however, the BET range matches the relative pressure range at which two molecular layers of interlayer water build up, as indicated by the first order basal spacings given in Table 8. Using the q_m values of the second group, the cross-sectional area of water molecule adsorbed on the clay mineral surfaces were calculated as described before. The results, ranging between $16.3\overset{o}{A}^2$ and $17.9\overset{o}{A}^2$, are listed in Table 9, along with the results obtained in the present study. The average of the values of cross-sectional area of adsorbed water molecule given in Table 9 is $17.0\overset{o}{A}^2$. The agreement between the BET-calculated cross-sectional area of adsorbed water molecules and the cross-sectional area determined from the spatial geometric arrangement of water molecules in an ice-like structure suggested by X-ray diffraction is quite striking. The cross-sectional area as determined by the BET method alone, can not be considered a proof for a particular spatial geometric arrangement of water molecules, but when combined with the results of X-ray diffraction study it constitutes a convincing experimental evidence.

Heat of adsorption
_____

The average heat of adsorption of the first adsorbed monomolecular layer of water less the heat of liquefaction was calculated by using equation 10 according to Brunauer (11), as follows:

Table 9. Cross-sectional molecular area and average heat of adsorption of monomolecular water adsorbed on montmorillonite, calculated from BET parameters listed

Mineral	BET parameters q_m	C	Cross-sectional area of adsorbed water molecule, s, $Å^2$	Average heat of adsorption less heat of liquefaction, E_1-E_L, K cal/mole According to Braunauer (11)	Corrected according to Clampitt and German (14)
Mississippi:					
Mg montmorillonite[a]	0.138	29	16.4	2.0	3.7
Ca montmorillonite[a]	0.130	23	17.3	1.9	3.6
Sr montmorillonite[a]	0.133	11	16.3	1.4	3.1
H montmorillonite[a]	0.129	10	17.9	1.4	3.1
Wyoming:					
Ca montmorillonite[a]	0.125	6	17.9	1.1	2.8
Ca montmorillonite[b]	0.130±0.005	6.7±0.8	17.3±0.7	1.1±0.1	2.8±0.1
Na montmorillonite[a]	0.135[c]	1.5	16.6	0.2	1.9
Na montmorillonite[b]	0.135[c]	1.4	16.6	0.2	1.9
California:					
Ca montmorillonite[a]	0.133	15	16.9	1.6	3.3

[a]Data of Hendricks et al. (32).

[b]Data of present study.

[c]Obtained by approximations described in the text.

$$E_1 - E_L = 2.303 \ RT \log C$$

$$= 2.303 \times 1.987 \times 297.5 \log C \ cal/mole$$

The values thus obtained were corrected according to Clampitt and German (14) by adding their correction value of 1700 cal (see p. 14). The results obtained are listed in Table 9.

$$E_1 - E_L = 2.303 \times 1.987 \times 297.5 \log C + 1700 \ cal/mole$$

Corrected $E_1 - E_L$ values for barium, lithium, sodium, potassium, cesium saturated Mississippi montmorillonite and sodium saturated California montmorillonite were also calculated and found to be 3.5, 3.6, 2.9, 2.8, 3.4 and 2.9 K cal/mole, respectively. The corrected values show reasonably good agreement with the value estimated from the isosteric heat of adsorption curve of Mooney et al. (49), evaluated by them from desorption isotherms of water on sodium montmorillonite by use of Clausius-Clapeyron equation. The value for $E_1 - E_L$ estimated from their curve at a moisture content of 3 percent is about 2.5 K cal/mole. The corrected values also showed agreement with the value estimated between 2 to 3 K cal/mole from Zettlemoyer et al. (61) heat of desorption curve for natural Wyoming bentonite (predominantly sodium montmorillonite). These comparisons show the reasonableness of the parameter C, which is a criterion for the justification of the use of BET theory as pointed out by Brunauer (10).

Free Energies of Wetting

The free energies of wetting defined by equation 8a were calculated by using equation 7. The numerical values of the $\int_0^1 \frac{q}{P/P_0} \, d \, (P/P_0)$ term of equation 7 were obtained by graphical integration (Figures 26 and 27) using the adsorption isotherm data given in Tables 2 and 4. By taking into account the limits of experimental errors discussed earlier, the numerical values for $\int_0^1 \frac{q}{P/P_0} \, d \, (P/P_0)$ were found to be 0.1893 $\pm$ 0.0104 and 0.4191 $\pm$ 0.0235 gram per gram of mineral for sodium and calcium montmorillonites, respectively. Substituting these values into equation 7 the free energies of wetting were calculated as follows:

$$\Delta F = - \frac{RT}{M\Sigma} \, 0.1893$$

$$= - \frac{8.314 \times 10^7 \times 297.5}{18.02 \times 748 \times 10^4} \times 0.1893$$

$$= - 34.76 \pm 1.91 \text{ erg/cm}^2$$

and

$$\Delta F = - \frac{RT}{M\Sigma} \, 0.4191$$

$$= - \frac{8.314 \times 10^7 \times 297.5}{18.02 \times 751 \times 10^4} \times 0.4191$$

$$= - 76.61 \pm 4.30 \text{ erg/cm}^2$$

for sodium and calcium montmorillonites, respectively. Substituting these values into equation 8a the following relationships were obtained

Figure 26. Plot for graphical integration of equation 7
for sodium montmorillonite

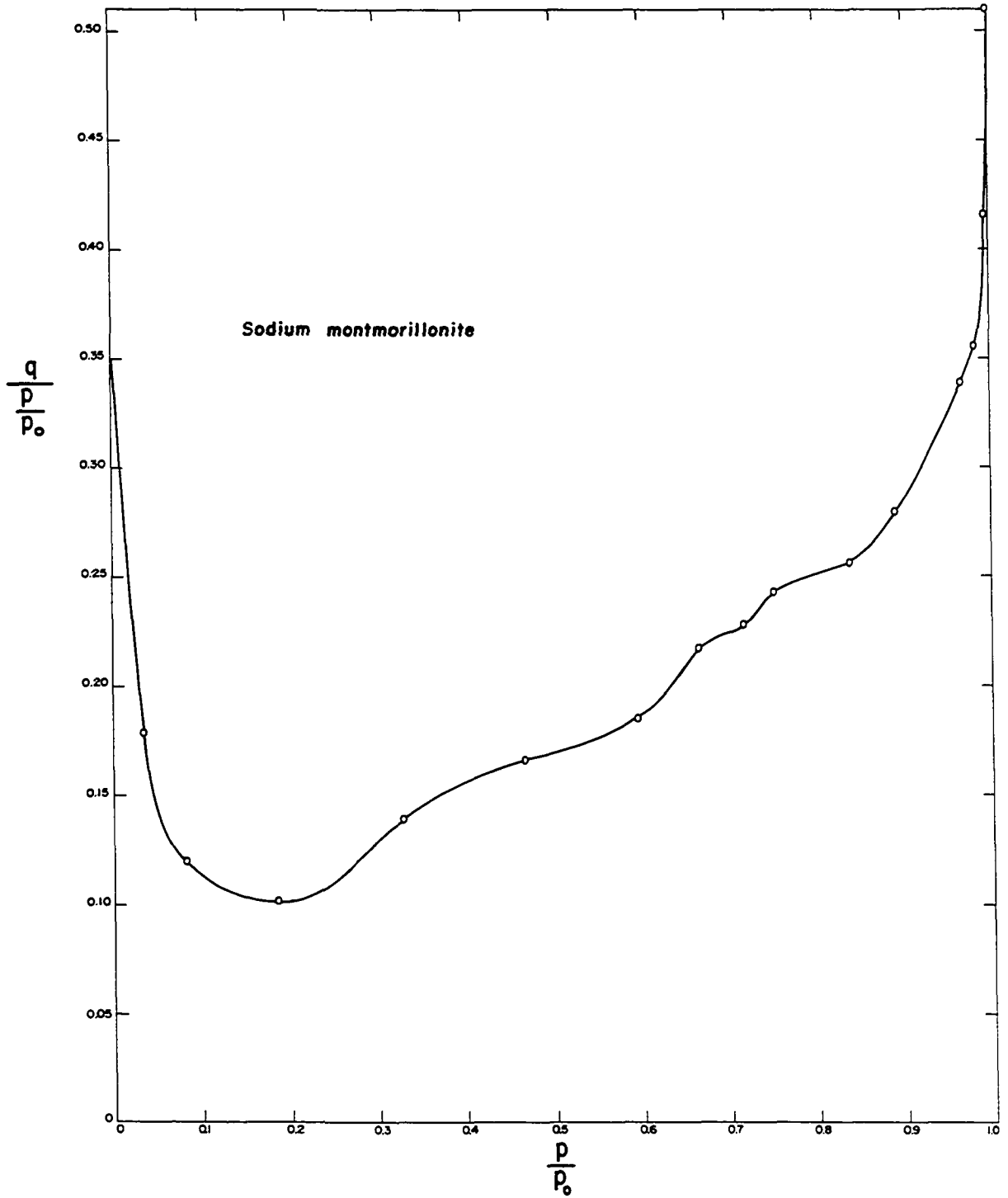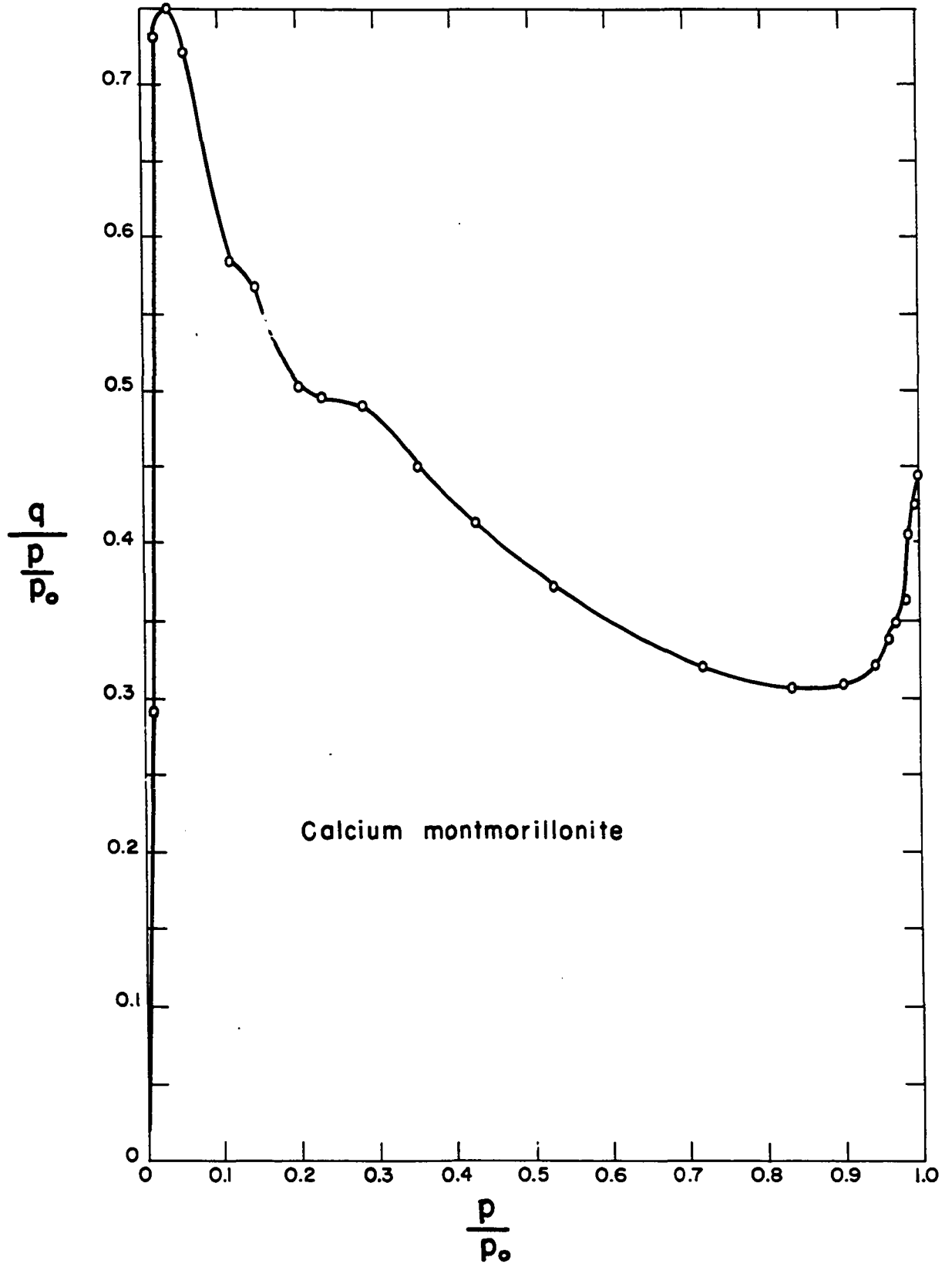Sodium montmorillonite

Figure 27. Plot for graphical integration of equation 7
            for calcium montmorillonite

Calcium montmorillonite

$$\Delta F_1 = (\gamma_{SL} - \gamma_{SO})_1 + a_1 \Delta V_1$$

$$= -34.76 \text{ erg/cm}^2 \text{ average surface}$$

and

$$\Delta F_2 = (\gamma_{SL} - \gamma_{SO})_2 + a_2 \Delta V_2$$

$$= -76.61 \text{ erg/cm}^2 \text{ average surface}$$

for sodium and calcium montmorillonites, respectively. If a is determinable from another experiment, for instance from nitrogen adsorption isotherms, and if it can be varied from one sample to another, for instance by using different sample preparation techniques, it would be possible to obtain two such equations for a mineral by performing two complete water adsorption isotherm experiments on the two samples of the mineral having different known values of a. The two equations could be solved simultaneously for $(\gamma_{SL} - \gamma_{SO})$ and ΔV. Since such information is not yet available only a qualitative treatment of the results of the free energies of wetting will be presented.

The lower negative value of the free energy of wetting for sodium montmorillonite compared to calcium montmorillonite implies that the sodium clay has less affinity for water. However, examination of the sketch in Figure 13 indicates that the change in potential energy (ΔV_1) with change in platelet separation distance for sodium montmorillonite is expected to be considerably higher than that for calcium montmorillonite (ΔV_2). A higher value of the $a\Delta V$ term in

equations 8a would be a reason for low negative free energy
of wetting of sodium montmorillonite. The α term, or the
interlayer fraction of the surface area, also is expected to
be higher for sodium than calcium montmorillonite. This is
indicated by its lower shrinkage limit (see Table 1), which
means that during drying, clay platelets approach one another
more closely before entry of air, indicating more layer-to-
layer and less edge-to-layer contact. As discussed earlier,
a high ΔV places the clay in a labile or unstable position
from a kinetic point of view. Therefore the organized water
molecules held on sodium montmorillonite can easily be
destroyed by the aggravation of water. Calcium montmoril-
lonite, favored by the high negative free energy of wetting
and being far from a labile position, tends to hold organized
water molecules.

CONCLUSIONS

Water vapor adsorption isotherm and X-ray diffraction data, some of which are from the literature, indicate the following:

1. The interlayer water take-up in montmorillonite is a multimolecular physical adsorption phenomenon, the maximum number of layers that can be adsorbed on interlayer surfaces being limited by the interaction of the montmorillonite platelets.

2. Calculations from BET theory indicate that the effective cross-sectional area of water molecules adsorbed on montmorillonite is about 17 $\overset{\circ}{A}^2$.

3. BET calculations give heats of adsorption of the first molecular layer of water on montmorillonite less the heat of condensation of water of between 2 and 4 K cal per mole as determined from the BET parameter C. This range agrees with the published values obtained by other methods including calorimetric determinations.

4. From the above, the BET theory appears applicable to the adsorption of water vapor on montmorillonite.

5. From use of Bangham's free energy equation, the free energy of wetting, defined as the free energy of immersion less the free energy change in particle interaction, is -34.76 ± 1.91 erg/cm^2 for sodium montmorillonite and -76.61 ± 4.30 erg/cm^2 for calcium montmorillonite.

6. X-ray d-spacing and BET parameter q_m requirements are met if:

(a) The configuration of the first molecular layer of interlayer water is similar to the hexagonal molecular configuration of the basal plane of ice. This structure fits upon that of the silicate surface. Each water molecule will be matched by an oxygen atom of the silicate surfaces if the montmorillonite platelet stacking is offset or rotated compared to muscovite stacking.

(b) The second molecular layer of interlayer water builds directly on top of the first layer.

(c) Additional water fits between first and second layer water molecules without appreciable expansion of the structure.

(d) Water to comprise third and fourth molecular layers fills between the hexagonal networks forming tetrahedrons with first and second layer water molecules, giving a structure similar to the complete unit cell of ice.

(e) The fifth molecular layer of water slips between the unit cell of ice and the montmorillonite silica surface, forming new hexagonal networks.

(f) The sixth molecular layer of water intrudes similarly to the fifth layer.

7. An evidence for offset stacking of clay mineral platelets, required if all water molecules are opposed by

silica layer oxygens (6a above), is a superlattice of the 001 reflection which was observed by X-ray diffraction.

8. The absence or extreme broadness of many hk reflections in montmorillonite compared to muscovite may also be due to offset stacking.

9. The organized interlayer water structure of calcium montmorillonite is thermodynamically and kinetically stable.

10. The organized interlayer water structure of sodium montmorillonite is thermodynamically less stable and kinetically unstable.

REFERENCES

1. Anderson, D. M. and Low, P. F. The density of water adsorbed by lithium-, sodium-, and potassium-bentonite. Proc. Soil Sci. America 22: 99-103. 1958.

2. Armbruster, M. H. A. and Austin, J. B. The adsorption of gases on smooth surfaces of steel. J. Am. Chem. Soc. 66: 159-171. 1944.

3. Bangham, D. H. The Gibbs adsorption equation and adsorption on solids. Trans. Faraday Soc. 33: 805-811. 1937.

4. Bangham, D. H. and Razouk, R. I. Adsorption and wettability of solid surfaces. Trans. Faraday Soc. 33: 1459-1463. 1937.

5. Barshad, I. The nature of lattice expansion and its relation to hydration in montmorillonite and vermiculite. Am. Mineralogist 34: 675-684. 1949.

6. Boyd, G. E. and Livingstone, H. K. Adsorption and energy changes at crystalline solid surfaces. J. Am. Chem. Soc. 64: 2383-2388. 1942.

7. Bradley, W. F. Density of water adsorbed on montmorillonite. Nature (London) 183: 1614-1615. 1959.

8. Brindley, G. W. Experimental methods. In Brown, G. The X-ray identification and crystal structures of clay minerals. pp. 1-50. London. Mineralogical Society. 1961.

9. Brown, G., editor. The X-ray identification and crystal structures of clay minerals. London. Mineralogical Society. 1961.

10. Brunauer, S. The adsorption of gases and vapors. Physical adsorption. Princeton. Princeton University Press. 1943.

11. Brunauer, S. Solid surfaces and solid-gas interface. Advances in Chemistry Series 33: 5-17. 1961.

12. Brunauer, S., Deming, L. S., Deming, W. E. and Teller, E. On a theory of van der Waals adsorption of gases. J. Am. Chem. Soc. 62: 1723-1732. 1940.

13. Brunauer, S., Emmett, P. H. and Teller, E. Adsorption of gases in multimolecular layers. J. Am. Chem. Soc. 60: 309-319. 1938.

14. Clampitt, B. H. and German, D. E. Heat of vaporization of molecules at liquid-vapor interfaces. J. Phys. Chem. 62: 438-440. 1958.

15. Craig, R. G., Van Voorhis, J. J. and Bartell, F. E. Free energy of immersion of compressed powders with different liquids. I. Graphite powders. J. Phys. Chem. 60: 1225-1230. 1956.

16. Deeds, C. T. and van Olphen, H. Density studies in clay-liquid systems. Advances in Chemistry Series 33: 332-339. 1961.

17. Demirel, T. and Enüstün, B. V. Free energies of wetting of minerals. I. Communications de la Faculte des Sciences de l universite d'Ankara 6: 1-19. 1957.

18. De Wit, C. T. and Arens, P. L. Moisture content and density of some clay minerals and some remarks on the hydration patterns of clay. Trans. 4th Intern. Congr. Soil Sci. 2: 59-62. 1950.

19. Docay, D. G., Fu, Y. and Bartell, F. E. Energetics of the adsorption of aliphatic amines by silica gel. J. Am. Chem. Soc. 73: 308-314. 1951.

20. Dushman, S. and Gaines, G. L. Jr. Sorption of gases and vapors by solids. In Lafferty, J. M. Scientific foundations of vacuum technique. pp. 376-434. New York, N. Y. John Wiley and Sons, Inc. 1962.

21. Emmett, P. H. and Brunauer, S. The use of low temperature van der Waals adsorption isotherms in determining the surface area of iron synthetic ammonia catalysts. J. Am. Chem. Soc. 59: 1553-1564. 1937.

22. Emmett, P. H., Brunauer, S. and Love, K. S. The measurement of surface area of soils and soil colloids by the use of low temperature van der Waals adsorption isotherms. Soil Sci. 45: 57-65. 1938.

23. Forslind, E. Crystal structure and water adsorption of clay minerals. Swedish Cement and Concrete Research Institute Bulletin 11: 1-20. 1948.

24. Forslind, E. Some remarks on the interaction between the exchangable ions and the adsorbed water layers in montmorillonite. Trans. 4th Intern. Congr. Soil Sci. 1: 110-113. 1950.

25. Foster, A. G. The sorption of condensible vapors by porous solids. I. The applicability of the capillary theory. Trans. Faraday Soc. 28: 645-657. 1932.

26. Fu, Y. and Bartell, F. E. Surface area of porous adsorbents. J. Phys. Chem. 55: 662-675. 1951.

27. Green-Kelly, R. Irreversible dehydration in montmorillonite. Clay Min. Bulletin (London) 1: 221-227. 1952.

28. Green-Kelly, R. Irreversible dehydration in montmorillonite. II. Clay Min. Bulletin (London) 2: 52-56. 1953.

29. Grim, R. E. Applied clay mineralogy. New York, N. Y. McGraw-Hill Book Company, Inc. 1962.

30. Grim, R. E. Clay mineralogy. New York, N. Y. McGraw-Hill Book Company, Inc. 1953.

31. Hendricks, S. B. and Jefferson, M. E. Structure of kaolin and talc-pyrophyllite hydrates and their bearing on water sorption of clays. Am. Mineralogist 23: 863-875. 1938.

32. Hendricks, S. B., Nelson, R. A. and Alexander, L. T. Hydration mechanism of the clay mineral montmorillonite saturated with various cations. J. Am. Chem. Soc. 62: 1457-1464. 1940.

33. Hodgman, C. D., Weast, R. C. and Selby, S. M. Handbook of chemistry and physics. Cleveland, Ohio. Chemical Rubber Publishing Co. 1958.

34. Inness, W. B. and Rowley, H. H. Relationship between the adsorption isotherm and the spreading force. J. Phys. Chem. 45: 158-165. 1941.

35. Jura, G. and Harkins, W. D. Determination of the decrease of free surface energy of a solid by an adsorbed film. J. Am. Chem. Soc. 66: 1356-1362. 1944.

36. Klug, H. P. and Alexander, L. E. X-ray diffraction procedures. New York, N. Y. John Wiley and Sons, Inc. 1954.

37. Lambe, T. W. The engineering behavior of compacted clay. Am. Soc. Civil Eng. Soil Mechanics and Foundations Division 84, No. 1655: 1-35. 1958.

38. Lambe, T. W. The structure of compacted clay. Am. Soc. Civil Eng. Soil Mechanics and Foundations Division 84, No. 1654: 1-34. 1958.

39. Livingston, H. K. Cross-sectional areas of molecules adsorbed on solid surfaces. J. Am. Chem. Soc. 66: 569-573. 1944.

40. Livingston, H. K. The cross-sectional areas of molecules adsorbed on solid surfaces. J. Colloid. Sci. 4: 447-457. 1949.

41. Macey, H. H. Clay-water relationship and the internal mechanism of drying. Trans. Ceramic Soc. (Engl.) 41: 73-121. 1942.

42. MacEvan, D. M. C. Montmorillonite minerals. In Brown, G. The X-ray identification and crystal structures of clay minerals. pp. 143-207. London. Mineralogical Society. 1961.

43. Mackenzie, R. C. Density of water sorbed on montmorillonite. Nature (London) 181: 334. 1958.

44. Marshall, C. E. The colloid chemistry of the silicate minerals. New York, N. Y. Academic Press, Inc., Publishers. 1949.

45. McBain, J. W. Colloid science. Boston, Mass. D. C. Heath and Company. 1950.

46. McBain, J. W. An explanation of hysteresis in the hydration and dehydration of gels. J. Am. Chem. Soc. 57: 699-700. 1935.

47. McBain, J. W. and Bakr, A. M. A new sorption balance. J. Am. Chem. Soc. 48: 690-695. 1926.

48. Mering, J. On the hydration of montmorillonite. Trans. Faraday Soc. 42B: 205-219. 1946.

49. Mooney, R. W., Keenan, A. G. and Wood, L. A. Adsorption
    of water vapor by montmorillonite. I. J. Am.
    Chem. Soc. 74: 1367-1371. 1952.

50. Mooney, R. W., Keenan, A. G. and Wood, L. A. Adsorption
    of water vapor by montmorillonite. II. J. Am.
    Chem. Soc. 74: 1371-1374. 1952.

51. National Research Council of the United States of
    America. International critical tables. Vol. 1.
    New York, N. Y. McGraw-Hill Book Company, Inc.
    1926.

52. Overbeek, J. Th. G. The interaction between colloidal
    particles. In Kruyt, H. R. Colloid science.
    Vol. 1. pp. 245-277. New York, N. Y. Elsevier
    Publishing Company. 1952.

53. Pauling, L. The nature of chemical bond. Ithaca, N. Y.
    Cornell University Press. 1960.

54. Rao, K. S. Hysteresis in sorption. V. Permanence,
    scanning, and drift of the hysteresis loop. J.
    Phys. Chem. 45: 522-531. 1941.

55. Road Research Laboratory, Department of Scientific and
    Industrial Research (Great Britain). Soil mechanics
    for road engineers. London. Her Majesty's Sta-
    tionery Office. 1954.

56. Russell, E. W. The interaction of clay with water and
    organic liquids as measured by specific volume
    changes, and its relation to the phenomena of
    crumb formation in soils. Phil. Trans. Roy. Soc.
    Series A, 233: 361-389. 1934.

57. Topping, J. Errors of observation and their treatment.
    London. The Institute of Physics. 1957.

58. Verwey, E. J. W. and Overbeek, J. Th. G. Theory of the
    stability of lyophobic colloids. New York, N. Y.
    Elsevier Publishing Company, Inc. 1948.

59. Williamson, W. O. The physical relationships between
    clay and water. Trans. Ceramic Soc. (Engl.) 50:
    10-34. 1951.

60. Winterkorn, H. F. The science of soil stabilization.
    Highway Research Board Bulletin 108: 1-24. 1955.

61. Zettlemoyer, A. C., Young, G. J. and Chessick, J. J.
     Studies of the surface chemistry of silicate min-
     erals. III. J. Phys. Chem. 59: 962-963. 1955.

ACKNOWLEDGEMENTS